Research Square

Preprints are preliminary reports that have not undergone peer review.
They should not be considered conclusive, used to inform clinical practice,
or referenced by the media as validated information.

Geomechanical Behavior of Filtered Iron Ore Tailings from the ‘Quadrilátero Ferrífero’ (Brazil) for Stack Disposal

Leonardo da Silva Machado

leonardo.d.machado@ufv.br

Universidade Federal de Viçosa

Eduardo Antonio Gomes Marques

Universidade Federal de Viçosa

António Viana da Fonseca

University of Porto

Bruno Guimarães Delgado

WSP Civils (United Kingdom)

Roberto Lopes Ferraz

Universidade Federal de Viçosa

Research Article

Keywords:

Posted Date: November 18th, 2026

DOI: https://doi.org/10.21203/rs.3.rs-9684385/v1

License: This work is licensed under a Creative Commons Attribution 4.0 International License.
Read Full License

Additional Declarations: No competing interests reported.

GEOMECHANICAL BEHAVIOR OF FILTERED IRON ORE TAILINGS FROM THE 'QUADRILÁTERO FERRÍFERO' (BRAZIL) FOR STACK DISPOSAL

Leonardo da Silva Machado, M.Sc.[1], Eduardo Antonio Gomes Marques, D.Sc.[2], António Viana da Fonseca, Ph.D.[3], Bruno Guimarães Delgado, Ph.D.[4], Roberto Lopes Ferraz, D.Sc.[5]

1 D. Sc. Researcher, Department of Civil Engineering, Universidade Federal de Viçosa, Avenida Peter Henry Rolfs, Campus Universitário, Viçosa, MG, Brazil, 36570-900. Email: leonardo.d.machado@ufv.br. ORCID: https://orcid.org/0000-0003-0192-5091 (Corresponding author).

2 Full Professor, Department of Civil Engineering, Universidade Federal de Viçosa, Avenida Peter Henry Rolfs, Campus Universitário, Viçosa, MG, Brazil, 36570-900. Email: emarques@ufv.br. ORCID: https://orcid.org/0000-0002-3476-8558.

3 Full Professor, Universidade do Porto, Rua Dr. Roberto Frias, Porto, Portugal, 4200-465. Email: viana@fe.up.pt. ORCID: https://orcid.org/0000-0002-9896-1410.

4 Principal Tailings Engineer and Researcher, WSP UK & Ireland; CONSTRUCT Research Centre, Rua Dr. Roberto Frias, Porto, Portugal, 4200-465. Email: bruno.delgado1@wsp.com. ORCID: https://orcid.org/0000-0002-6847-1314.

5 Associate Professor, Department of Civil Engineering, Universidade Federal de Viçosa, Avenida Peter Henry Rolfs, Campus Universitário, Viçosa, MG, Brazil, 36570-900. Email: rlferraz@ufv.br. ORCID: https://orcid.org/0000-0001-7034-9169.

ABSTRACT

This study seeks to determine the geomechanical behavior of iron ore tailings from the 'Quadrilátero Ferrífero', Brazil, in a wide range of stresses. An extensive geotechnical investigation campaign was conducted to obtain the normal compression lines (NCLs) and critical state lines (CSLs) of the material. To this end, oedometric consolidation tests and drained (CID) and undrained (CIU) isotropic triaxial tests were performed with consolidation stresses ranging from 100 to 4500 kPa. Curvilinear behavior was observed for both the NCL and CSL in the $e - ln\, p'$ plane, mainly under high-stress conditions (p' above 6000 kPa), which is explained by the breakage of sandy particles, predominantly silica (SiO_2). To verify the granulometric change in the material, the particle breakage index (B_g) and changes in the grain shape were evaluated by scanning electron microscopy (SEM) tests and image interpretation. Based on these results, a division of the CSL of the tailings in the $e - ln\, p'$ plane was proposed into ranges with geomechanical behavior of strain hardening and fabric change. In addition, calibrations of the dilatancy parameters (N_{tc} and χ_{tc}) of the material were performed, from which fabric effects resulting from the initial void ratios of the samples were observed. Finally, an S-CPTu test was performed on experimental dry stacking, where the relationship between the shear modulus (G_0) and the average effective stress (p') was calibrated. The values of the geomechanical parameters obtained for the material studied were consistent with the results of other studies on iron ore tailings.

KEYWORDS: Soil mechanics of critical states; Shear strength; Stress path; Tailings disposal; Laboratory tests.

PRACTICAL APPLICATION

The 'Quadrilátero Ferrífero' region in Minas Gerais is one of the key areas for iron ore mining in Brazil. Millions of tons of products are generated annually, as are millions of tons of tailings. For a long time, the mining industry has used dams as the main method of tailings disposal. However, owing to accidents that have occurred in the last decade and the emergence of restrictive (Brazilian) legislation for these structures, it was necessary to adopt different alternatives for material disposal. Given this scenario, dry stacking was selected as a technically practical solution. However, owing to the large volume of tailings to be disposed of, tall structures have been designed more often. Therefore, conducting more in-depth studies on the

geomechanical behavior of iron ore tailings subjected to high stress is essential to increase understanding of those materials under high stress, to obtain dependable parameters and, thus, supporting safer projects.

1. INTRODUCTION

Tailings are materials with no economic value, generated during the mineral processing process (ANM 2025). Unlike soils, which result from geological change, pedological processes and the weathering of rocks, tailings are formed by industrial processes – such as crushing, grinding, and others. The growing demand for iron ore for steel production, driven by global industrial development (Zhang 2023), has resulted in ever-increasing volumes of tailings generated by mining activities.

Traditionally, in Brazil, these tailings are disposed of in dams, a practice that, although economically viable and technically well known, has been associated with significant risks when the upstream raising method is used. This fact is evidenced by environmental and civil disasters of great impact, such as those that occurred in Mariana (2015) and Brumadinho (2019) (Arroyo and Gens 2021; Consoli et al. 2024a; Delgado et al. 2025; Dos Santos et al. 2020; Islam and Murakami 2021; Lyu et al. 2019; Morgenstern et al. 2016; Robertson et al. 2019; Viana da Fonseca et al. 2021; Viana da Fonseca et al. 2022; Viana da Fonseca 2026). These events prompted a review of Brazilian legislation and the search for safer and more sustainable technological alternatives for tailings disposal (ANM 2025).

In this context, dry stacking has been identified as a promising solution. This technique consists of filtering the tailings slurry to a moisture content that allows them to be stacked and compacted, forming piles with less potential associated damage (PDA) than conventional dams, which retain large volumes of water. Thus, these structures can be identified as large stacks and offer better safety conditions (Amoah et al. 2018).

Current tailings dry stacking designs call for stacks that are more than 160 m high, which means that these materials are subjected to high stresses (Cacciuttolo and Valenzuela 2022; Corrêa de Oliveira et al. 2025).

In addition, mining companies are currently studying the possibility of constructing stacking structures with heights up to 350 m of tailings. Studies such as the one presented by Assis Júnior (2026) support this assessment. Considering the evolution of the K_0 value at high stress levels, as indicated in the results of this study, at this height, stress levels exceed 6000 kPa (indicated in the results as the linear limit of the CSL in this study). In addition to its practical application, this work is also related to the research interest in the geomechanical behavior of these materials, even at stresses higher than

69 those encountered in these structures. Therefore, understanding the geomechanical behavior of iron ore tailings under high
70 stress is essential for the development of projects and to ensure structural safety.

71 Even though the geomechanical behavior of the tailings can be interpreted using soil mechanics principles, the material
72 exhibits certain characteristics distinct from those of natural soils and therefore requires detailed investigation, including
73 specific laboratory procedures used and described in this study. Consequently, tailings are classified as non-conventional
74 (non-textbook) geomaterial, with properties strongly influenced by the local geology, ore processing technology, and
75 disposal methods. In addition, the 'Quadrilátero Ferrífero' region is one of the world's major iron ore producers, located in
76 a tropical country with high rainfall rates, where recent tailings dam failures demand strict rigor in understanding the
77 expected behavior of filtered tailings stacks.

78 Furthermore, critical state soil mechanics (CSSM) offers a robust theoretical framework for analyzing the behavior of soils
79 under different loading conditions and should be used for evaluating these cases (Delgado et al. 2023).

80 The critical state line (CSL) defines the final state in which the soil deforms continuously without changing volume or stress.
81 This line is often considered linear in the void ratio (e) versus the logarithm of the mean effective stress ($ln\ p'$) plane
82 (Jefferies and Been 2016). Recent research has shown that the CSL may exhibit non-linear or curvilinear behavior, especially
83 in iron ore tailings from the 'Quadrilátero Ferrífero' region (Delgado et al. 2025; Delgado et al. 2023; Rios et al. 2025; Silva
84 et al. 2024a; Silva et al. 2024b). This non-linearity can be attributed to phenomena such as particle breakage under high
85 stress, which alters the particle size/morphology of the material and thus the mechanical properties of the tailings (Corrêa de
86 Oliveira et al. 2025; Delgado et al. 2025; Delgado et al. 2023).

87 In this context, the present study investigates the geomechanical behavior of iron ore tailings from the 'Quadrilátero Ferrífero'
88 region, for which experimental data and characterization remain limited in the literature. Specifically, the material originates
89 from the beneficiation of hematitic ore, unlike most tailings investigated in previous studies, which predominantly focus on
90 materials generated from itabirite processing.

91 This difference in origin is associated with distinctive characteristics of the investigated tailings, particularly their higher
92 fines content and elevated concentration of iron oxides (Fe_2O_3), which contribute to geomechanical behavior differing from
93 that reported for other iron ore tailings. Furthermore, this investigation is particularly relevant given the generation of tens

of millions of tonnes of this material annually and the consequent need for appropriate solutions for its disposal in tailings storage facilities.

To improve the understanding of this material, an extensive experimental program was conducted, including isotropic triaxial compression tests at consolidation stresses ranging from 100 to 4500 kPa and oedometer consolidation tests to characterize the geomechanical parameters and evaluate the relationships between the compression curves, the critical state line, and the normal compression line (NCL).

Additionally, strength tests were performed using advanced triaxial testing procedures for tailings, consistent with current international practices (Viana da Fonseca et al. 2021), together with interlaboratory comparisons to assess the consistency of the experimental results. The potential for particle breakage and its relationship with changes in the CSL were investigated by analyzing variations in grain-size using the particle breakage index (B_g) proposed by Marsal (1967), as well as changes in particle dimensions assessed through scanning electron microscopy (SEM).

The experimental program was complemented by a seismic piezocone penetration test (S-CPTu) conducted in an 11.5 m – high experimental stack compacted under conditions representative of those expected in the design, aiming to determine the maximum shear modulus (G_0) in situ. Overall, this comprehensive investigation contributes to a better understanding of the geomechanical behavior of hematitic iron ore tailings under different stress levels, providing insights into the influence of particle breakage on the CSL, the characterization of in situ stiffness properties, and the geomechanical assessment of tailings storage facilities.

2. MATERIALS

The composition and characteristics of tailings vary significantly depending on the geological origin of the ore, the beneficiation process used, and the final particle size of the material. Iron ore tailings are often composed of a mixture of fines and coarser materials, with a general predominance of silt and sand particles (Faria 2022). Table 1 illustrates the wide variability in the physical characteristics and composition of iron ore tailings from the ‘Quadrilátero Ferrífero’ (from the most recent research to the least recent).

Table 1 Variability in the characteristics of iron ore tailings from the 'Quadrilátero Ferrífero' region

Iron ore tailings	Fines content < 0.06 mm (%)	G_s	e_{max}	e_{min}	Fe oxide (%)	Si oxide (%)
Viana da Fonseca (2026); Viana da Fonseca et al. (2023); Viana da Fonseca et al. (2022)	~58.00 – 83.00	3.94 – 5.00	1.22 – 1.40	0.89 – 0.48	96.00 – 67.00	-
Coutinho et al. (2025)	50.00	2.93	-	-	-	-
Consoli et al. (2025)	98.00	3.71	2.32	0.64	54.00	28.00
Corrêa de Oliveira et al. (2025)	33.30 – 51.70	2.97 – 3.05	0.99 – 1.28	0.51	17.20 – 20.90	76.2 – 78.40
De Andrade et al. (2025)	55.00	3.12	-	-	23.00	61.50
Delgado et al. (2025)	36.49	4.99	1.22	0.48	95.23	2.23
Dias Neto et al. (2025)	79.50 – 62.40	3.21 – 3.36	-	0.47	-	-
Rios et al. (2025)	41.00	3.01	1.04	0.53	-	-
Ccotohuanca et al. (2024)[a]	0.00 – 98.70	2.78 – 4.89	1.09 – 1.37	0.48 – 0.71	1.70 – 87.60	-
Consoli et al. (2024a); Silva et al. (2024a)	48.00	3.05	1.28	0.36	20.90	76.20
Consoli et al. (2024b)	38.60 – 86.19	2.83 – 4.02	1.08 – 1.09	0.50 – 0.57	-	-
Silva et al. (2024b)	~37.50	3.06	1.28	0.36	17.20	78.40
Faria et al. (2024); Faria (2022); Eloi (2021)	~80.00	4.55	-	-	-	-
Carneiro et al. (2023)	~83.00	3.21	-	-	-	-
Delgado et al. (2023)	~17.00	2.85	-	-	-	-
Santana (2022)	~24.00	-	-	-	-	-
Carneiro (2021); Oliveira (2021)	83.00 – 94.00	3.18 – 3.22	1.18	0.60	-	-
Reid et al. (2021)[b]	~54.00	2.78	-	-	-	-
Robertson et al. (2019)	~92.00 – 100.00	2.71 – 5.22	-	-	59.30 – 70.90	12.00 – 28.50
Morgenstern et al. (2016)	~32.00 – 98.00	2.38 – 4.34	-	-	73.80	19.20

[a] This study considers the consolidation of various data on the characteristics of tailings; [b] The study considers tests of the same material in several laboratories.

Studies have shown that the particle size distribution, actual grain density, void ratio, plasticity, morphology, and mineralogy are deciding factors in the geomechanical behavior of tailings (Bedin et al. 2012; Ccotohuanca et al. 2024; Ji et al. 2024; Macedo and Vergaray 2022; Schnaid et al. 2013; Velten et al. 2025; Viana da Fonseca et al. 2021; Viana da Fonseca and Delgado 2026). In this regard, attention is given to the proportion of fines, the actual specific gravity of the grains, the morphology and mineralogy of particles, which are characteristics that somewhat vary within the same mine due to changes in the mining front and geology and can result in significant changes in this behavior (Ji et al. 2024; Velten et al. 2025).

The material under study is of iron ore tailings generated by the processing of friable hematite, which is commonly mined in the 'Quadrilátero Ferrífero' region, making it representative of the materials found in many large dry-stacked tailings deposits in the region. This same material has already been the subject of studies on geotechnical characterization and hydraulic behavior of percolation and suction (Carneiro et al. 2023; Dias Neto et al. 2024; Dias Neto et al. 2025), which have been complemented by this research, with the performance of mechanical tests. In the present work, studies were conducted to evaluate the physical evolution of these tailings and to provide additional information across a wider range of stresses, the implications of which are related to the critical behavior of the material under drained and undrained conditions.

Thus, the choice of these tailings as the object of study is strategic, given the relevance of the region for global iron mining (Cavalcanti et al. 2023) and the need for a better understanding of the geomechanical behavior of tailings when disposed of in large and very high dry stacks.

Initially, several tests were performed to characterize the material, as shown in Table 2. This table also presents the standards used in performing all the tests. Significantly, these characterization tests were performed in a Brazilian commercial geotechnical laboratory, as were the CID and CIU triaxial tests. The exceptions were the validation tests (triaxial) with lubricated bases and guided pistons, which were performed at the Geotechnical Laboratory of the Faculty of Engineering of the Universidade do Porto (CID – ID 91 and CID – ID 92), Portugal. The additional triaxial tests performed at FEUP, using lubricated bases and guided pistons, were intended to validate the results obtained from the initial tests conducted at the Brazilian commercial laboratory, which did not employ these procedures. The purpose was not to compare the two testing methodologies, but rather to assess the consistency of the experimental results.

Table 2 Geotechnical tests performed for this study

Geotechnical testing	Technical standard
Grain size distribution	ASTM D6913/D6913M-17; ASTM D7928-21E01
Liquid limit, plasticity limit, and plasticity index	ASTM D4318-26
Specific gravity (G_s)	ASTM D854-23
Maximum and minimum void ratio	ASTM D4253-16; ASTM D4254-16; JSCE-G 582
Compaction test – Proctor method	AASHTO T99; AASHTO T180; ASTM D698-12 ; ASTM D1557-12
Scanning electron microscopy (SEM)	-
X-ray fluorescence (XRF)	-
Energy dispersive X-ray spectroscopy (EDS)	-

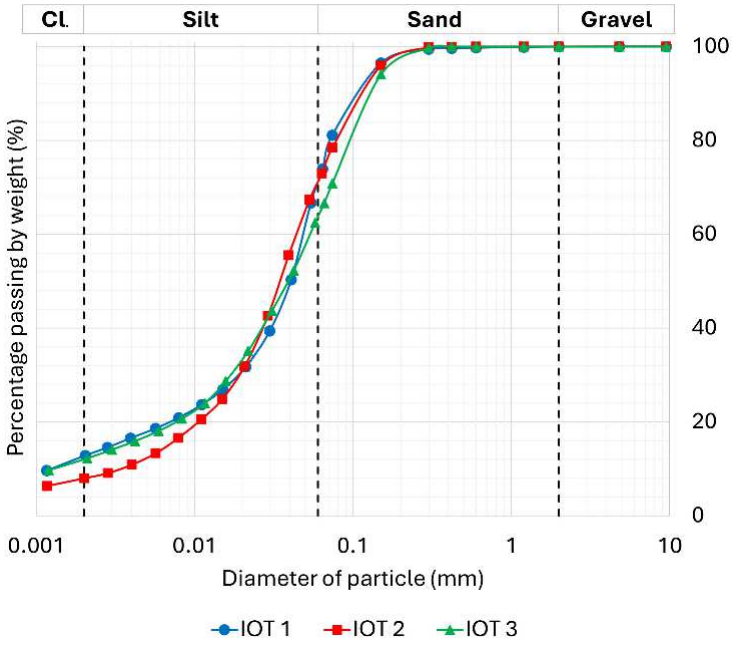
Geotechnical testing	Technical standard
One-dimensional consolidation (oedometric consolidation)	ASTM D2435/D2435M-25
Isotropically drained consolidated triaxial compression	Head (1982); ASTM D7181-20
Isotropically undrained consolidated triaxial compression	Head (1982); ASTM D4767-11
S-CPTu	ASTM D5778-20; ASTM D7400/D7400M-19

146

147 **2.1. BASIC GEOTECHNICAL, MINERALOGICAL, AND CHEMICAL CHARACTERIZATION**

148 First, particle size distribution tests were performed on the material. For this purpose, three samples of tailings were collected
149 from the mining company's storage yards after filtration [named as IOT (iron ore tailings) 1, IOT 2, and IOT 3] to verify the
150 uniformity of the material under study. This uniformity was verified, and the material was characterized as sandy silt (USCS)
151 (ASTM 2016), as shown in Fig. 1.

152 **Fig. 1** Particle size distribution curves of the iron ore tailings under study

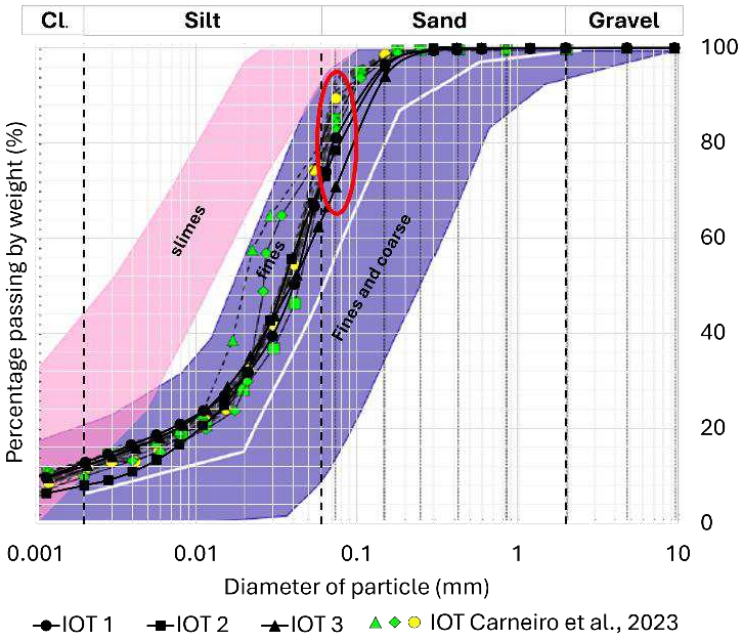


153

154 In addition, as shown in Fig. 2, the material was checked for compliance with the fines content of the tailings, as proposed
155 in the studies conducted by Carneiro et al. (2023). Based on this assessment, the material fell within the range of fine iron
156 ore tailings rather than clay tailings (a classification specific to the mining industry). It should be noted that, comparatively,
157 the tailings under study have a lower amount of fines (~13% to 16% less) than the material from the same mine and with the

158 same processing, as used in the studies by Dias Neto et al. (2025); Dias Neto et al. (2024); and Carneiro et al. (2023). This
159 variation suggests changes in the type of material mined, which, as presented later, may influence the geomechanical
160 characteristics of the tailings.

161 **Fig. 2** Comparison of the average particle size distributions (Adapted from Carneiro et al. 2023)

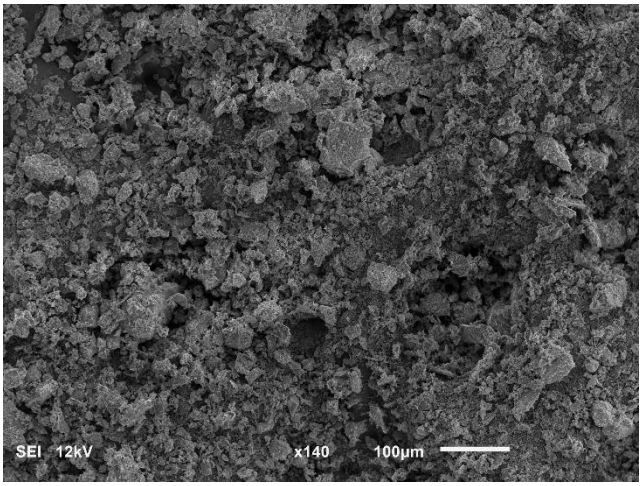


162

163 The results of the scanning electron microscopy (SEM) tests are shown in Figs. 3a and 3b. These tests were performed at
164 the SEM Laboratory of the Universidade Federal de Viçosa (UFV), where the presence of angular sand particles surrounded
165 by a tangle of flocculated silt particles with low sphericity was identified (based on Fletcher et al. 2003). As presented in
166 Table 3, the tailings under study are composed of iron oxide, represented by smaller grains, and silica oxide, represented by
167 larger grains. These results are consistent with the observations of Dias Neto et al. (2025), who reported that the existence
168 of macro and micropores in tailings is influenced by the chemical composition of the material.

Fig. 3 Scanning electron microscopy (SEM): (a) 100 μm; (b) 5 μm

(a)



(b)

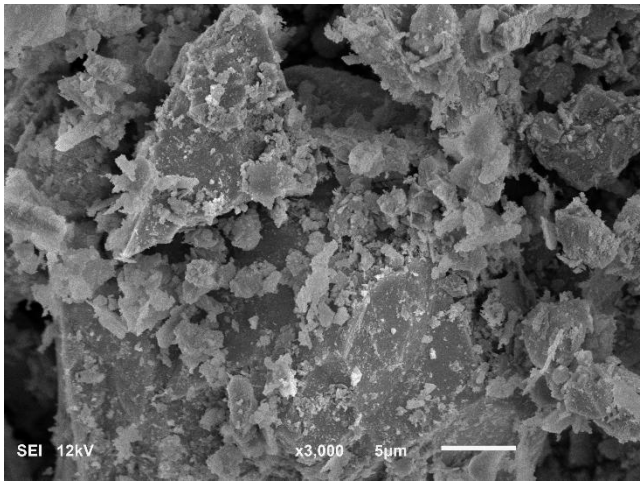
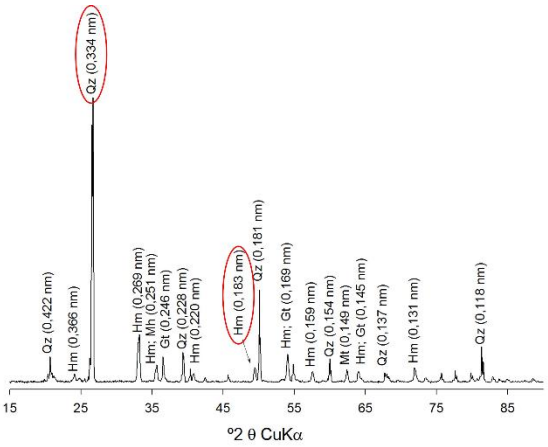


Fig. 4 and Table 3 show the results of X-ray fluorescence (XRF) and energy dispersive X-ray spectroscopy (EDS) tests, which were also performed to characterize the tailings. The first test was performed at the Civil Construction Laboratory of the Universidade Federal de Ouro Preto, and the second test was performed in conjunction with SEM at UFV.

In these tests, a large amount of silica (SiO_2) – 34.04% – was identified as sandy material, and hematite (Fe_2O_3) – 55.02% – was identified as silty material in the SEM, as mentioned above. The XRF data (Table 3) show a good relationship with the granulometric curves and percentages presented in Fig. 1. Furthermore, an interesting point is the high percentage of iron oxide in the sample, which could even be characterized as a material with potential for future mineral recovery, given that these values are close to the maximum percentage limits for iron ore tailings previously studied, as well as for mineral

deposits in the region (Consoli et al. 2025; Vick 1990). It is important to note that even though this percentage is high, it is lower than the percentages for the materials studied by Viana da Fonseca (2026).

Fig. 4 Energy dispersive X-ray spectroscopy (EDS)



Qz – quartz; Hm – hematite; Gt – goethite.

Table 3 X-ray fluorescence (XRF)

Element	Percentage (%)
Al_2O_3	9.28
CaO	0.03
Eu_2O_3	0.24
Fe_2O_3	55.02
MnO	0.69
P_2O_5	0.20
K_2O	0.07
SiO_2	34.04
TiO_2	0.30

The results of the tests that were used to determine the liquid limits, plasticity index, actual specific gravity of the grains (G_s), and minimum (e_{min}) and maximum (e_{max}) void ratios are presented in Table 4, indicating values consistent with other iron ore tailings from the 'Quadrilátero Ferrífero' region and used in previous studies (Carneiro 2021; Carneiro et al. 2023; Consoli et al. 2024a; Corrêa de Oliveira et al. 2025; Coutinho et al. 2025; De Andrade et al. 2025; Dias Neto et al. 2025;

191 Oliveira 2021; Silva et al. 2024a, Viana da Fonseca 2026). Among the results obtained in the tests, a high G_s value, of 3.27,
192 is observed, which is justified by the high amount of Fe_2O_3 in the sample, in addition to a large portion of fines (passing
193 through the #200 sieve), 69.15%.

194 **Table 4** Physical properties

Property	Result
Fines content (%)	69.15
Specific gravity, G_s	3.27
Average particle diameter, D_{50} (mm)	0.04
Coefficient of curvature,Cc	6.68
Coefficient of uniformity,Cu	40.28
Plasticity index (%)	4.00
Maximum void ratio,e_{max}	1.13
Minimum void ratio,e_{min}	0.18

195

196

197 ## 3. METHODS

198 As mentioned earlier, conducting tests for the geomechanical characterization of tailings requires specific details that enable
199 an adequate assessment of the material's behavior. The methodology used in this study to perform triaxial tests is outlined
200 below, in line with engineering best practices, to obtain the material's purely intrinsic characteristics.

201 For triaxial tests, the samples were molded via moist tamping method and compacted into six uniform layers with
202 undercompaction (Jefferies and Been 2016). Molding was performed in a cylinder, with controlled deposition and
203 compaction of the layers, to minimize the vertical heterogeneity of the test sample, in accordance with the guidelines
204 proposed by Viana da Fonseca et al. (2021).

205 Compaction was performed using guided pistons, the effort of which was previously adjusted to achieve the target void ratio
206 to be achieved, in line with the concept of initial state control recommended by Ladd (1978) and widely adopted in recent
207 studies that employ moist tamping (Viana da Fonseca et al. 2021).

208 Fig. 5a, 5b, and 5c show examples of the equipment used, and the test samples were molded via the moist tamping method.

Fig. 5 Molding of the test sample: (a) socket; (b) mold; (c) test sample

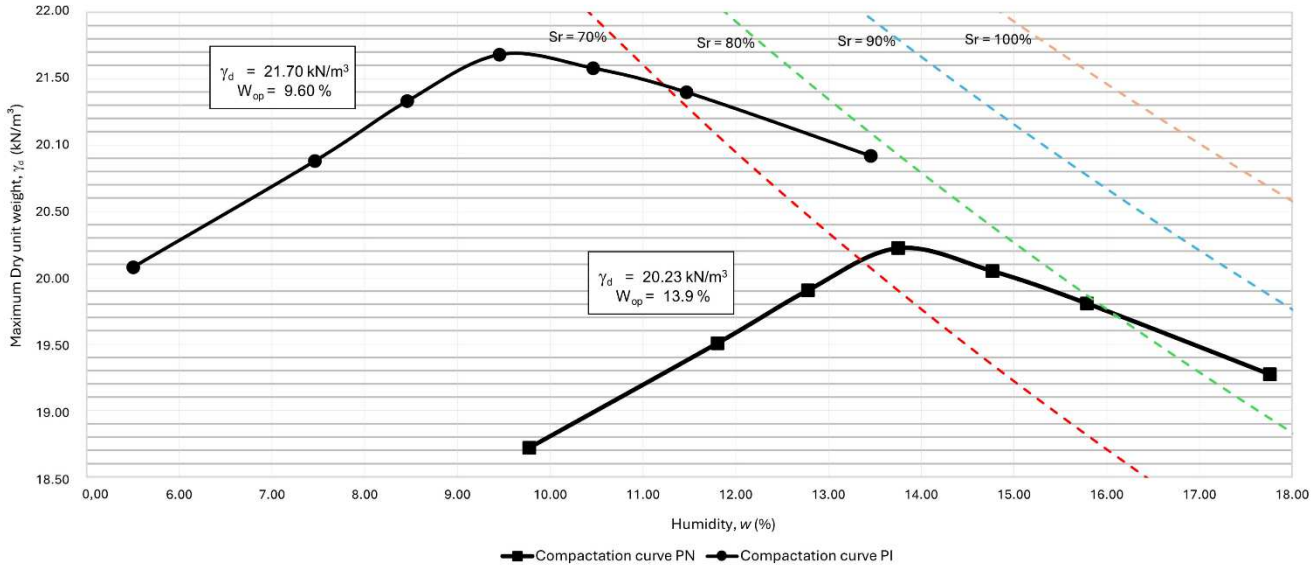
(a)  (b)  (c) 

The moist tamping method was used to mold the samples, with strict control of the void ratio and moisture content. Initially, problems relating to a lack of uniformity or high deformation of the test samples were initially observed during the sample preparation stage, for void ratios above 0.68. Thus, it was necessary to consider samples with void ratios below 0.68 for the tests. This void distribution is consistent with the maximum value of the state parameter (ψ), as indicated by Jefferies and Been (2016), Eq. (1), and is related to the critical stress ratio (M_{tc}), dilatancy (N), and dilatancy coefficient (χ).

$$\psi < M_{tc} \,/\, \chi \; x \; (1 + N) \qquad \text{(Eq. 1)}$$

Importantly, the variations in the void and moisture content indices of the molded samples were determined according to the relationships defined in the Proctor curves with normal effort (PN) and intermediate effort (PI) and the respective moisture content of the sample (Fig. 6). This methodology aims to follow the references of the technological control activities that are performed in the field for the implementation of tailings dry stacking, according to the field representativeness indicated by Coop (1999); Coop (2004); Ishihara (1996). Importantly, the void ratio ranges were also consistent with the studies and methodologies presented by Viana da Fonseca et al. (2021).

Fig. 6 Compaction curves for field technology control



After molding, saturation was started until the samples presented Skempton's B parameter values (Skempton 1954) greater than 0.98, according to the criteria set by ASTM standards. For the consolidation stage, the tests followed consolidation stress levels of 100, 200, 400, 800, 1500, 2000, 3000, 4000, and 4500 kPa.

For the tests performed at FEUP, the upper and lower ends of the test samples were prepared with lubricated bases, consisting of silicone membranes associated with a thin layer of silicone grease, to reduce the effects of friction on the plates and promote a more uniform distribution of stresses.

Axial loading was applied via pistons. For the tests performed at FEUP, these pistons were guided, ensuring that the force was applied in an axially aligned manner and minimizing eccentricity effects on the sample (Viana da Fonseca et al. 2021). In addition, at the end of these tests, the samples were frozen to determine the final void ratios.

A total of eighteen specimens were molded for each of the five void ratios. Half of the test samples were sheared in a drained manner, and the other half were sheared in an undrained manner. IOT was evaluated under drained (CID) and undrained (CIU) isotropic conditions.

The tests were conducted up to a maximum axial strain (εa) of 20%. The triaxial tests conducted at a commercial laboratory present void ratio calculated using the Verdugo (1992) method. These results were validated by tests conducted at FEUP (ID–91 and ID–92) using frozen samples (Viana da Fonseca et al. 2021).

The looser samples (higher void ratios) from the drained tests were used to characterize the isotropic NCL (Pacheco Silva 1970; Pestana 1996) and the CSL and associated parameters (Γ – void ratio with p' at 1 kPa and λ – compression index, for the SemiLog/Logarithm CSL [Eq. (2)] and a, b, and c as variables for the PowerLaw CSL [Eq. (3)]. Loose samples under undrained conditions were used to confirm the behavior of the CSL.

$$e_{CSL} = \Gamma - \lambda \, x \, ln \, p' \quad \text{(Eq. 2)}$$

$$e_{CSL} = a - b \, x \, (p' / 100)^c \quad \text{(Eq. 3)}$$

After the shearing, some samples from the commercial laboratory exhibited localizing, that is, the formation of shear bands, a condition that was directly observable in the sample's deformation. This condition makes it impossible to use the sample to define the CSL. In addition to the earlier specimens that were not used to define the CSL due to localization, those samples that did not reach the critical state were identified and excluded from the analyses.

As shown by Jefferies and Been (2016), to verify the critical condition of drained samples, the following conditions of dilatancy (D), Eq. (4), and distortional deformation (εq), Eq. (5), must be met.

$$D = 0 \quad \text{(Eq. 4)}$$

$$\delta D / \delta \varepsilon q = 0 \quad \text{(Eq. 5)}$$

The classic criterion (Roscoe et al. 1958) used for undrained tests considers that the critical state is reached once the stresses (p' and q) [Eq. (6) and Eq. (7)] and pore pressure (u) [Eq. (8)] have stabilized.

$$\delta p' / \delta \varepsilon q = 0 \quad \text{(Eq. 6)}$$

$$\delta q / \delta \varepsilon q = 0 \quad \text{(Eq. 7)}$$

$$\delta u / \delta \varepsilon q = 0 \quad \text{(Eq. 8)}$$

Based on the CSL obtained, two additional complementary CID tests (100 and 2500 kPa, ID 91 and ID 92, respectively) were performed at FEUP, according to the methodology of Viana da Fonseca et al. (2021), with the aim of evaluating the data previously obtained in commercial laboratories.

The dense samples (lower void ratios) from drained tests were important for defining the volumetric coupling parameter of dilatancy (N_{tc}) and the dilatancy coefficient (χ_{tc}) for triaxial compression (Jefferies and Shuttle 2002). In addition, the

compilation of specimens that reached the critical state was used to find the slope of the straight line of the $q - p'$ stress paths (M_{tc}).

The samples for the oedometer consolidation tests were molded in the laboratory via compaction and a press, considering a previously defined soil volume, which was compressed until the sample reached the final height specified for the test. The procedure was conducted in a controlled manner to ensure that the initial void ratio was compatible with that adopted in triaxial tests ASTM (2011a). For the oedometric consolidation tests, the five samples were loaded to the stage of maximum effective vertical stress (σ'_v) and subsequently unloaded through the same loading stress levels in reverse order.

Oedometric consolidation tests were performed with variations in the void ratios of the loading stage between 0.64 and 0.39 (Table 5), and triaxial tests were performed under drained and undrained isotropic conditions with void ratio variations between 0.63 and 0.36 after the sample consolidation stages (Table 6).

Table 5 Characteristics of the oedometric compaction tests

ID	Type of test	σ'_v (kPa)	Proctor and moisture content	Void ratio for the loading stage	Void ratio for the unloading stage
1 to 9	Oed	100 to 4500	PN 13.9%	0.59	0.44
10 to 18	Oed	100 to 4500	PN 15.9%	0.61	0.45
19 to 27	Oed	100 to 4500	PN 16.9%	0.64	0.46
28 to 36	Oed	100 to 4500	PI 11.5%	0.50	0.39
37 to 45	Oed	100 to 4500	PI 13.5%	0.55	0.42

Table 6 Characteristics of the triaxial tests

ID	Type of test	σ'_c (kPa)	Proctor and moisture content	Initial void ratio (e_0)	Selected samples (ID)
1 to 9	CID[a]	100 to 4500	PN 13.9%	0.62 to 0.61	2; 8
10 to 18	CID[a]	100 to 4500	PN 15.9%	0.65	12; 17; 18
19 to 27	CID[a]	100 to 4500	PN 16.9%	0.68 to 0.67	19; 22; 23; 24
28 to 36	CID[b]	100 to 4500	PI 11.5%	0.53	28; 29; 30; 31
37 to 45	CID[b]	100 to 4500	PI 13.5%	0.56	37; 38
46 to 54	CIU[a]	100 to 4500	PN 13.9%	0.62 to 0.61	49; 50; 51; 54
55 to 63	CIU[a]	100 to 4500	PN 15.9%	0.66 to 0.64	55; 56

ID	Type of test	σ'_c (kPa)	Proctor and moisture content	Initial void ratio (e_0)	Selected samples (ID)
64 to 72	CIU[a]	100 to 4500	PN 16.9%	0.68 to 0.67	-
73 to 81	CIU[a]	100 to 4500	PI 11.5%	0.53	74; 75
81 to 90	CIU[a]	100 to 4500	PI 13.5%	0.53	83
91	CID[c]	100	PN 13.9%	0.67	91
92	CID[c]	2500	PN 13.9%	0.65	92

277 [a] Loose samples used for CSL calibration; [b] Dense samples used for dilatancy parameter calibration; [c] Samples evaluated at
278 FEUP for CSL validation in the $e - ln\, p'$ plane.

279 Finally, the S-CPTu tests were performed on an experimental dry stack (Fig. 7), which was approximately 11.5 m high and
280 constructed using the same tailings as in the laboratory tests. The aim was to determine the $G_0 - p'$ ratio by measuring shear
281 waves at levels below the dry stack's water level. These tests were performed using Pagani TG 63-150 equipment supplied
282 by a commercial company.

283 **Fig. 7** Experimental dry stacking

284 

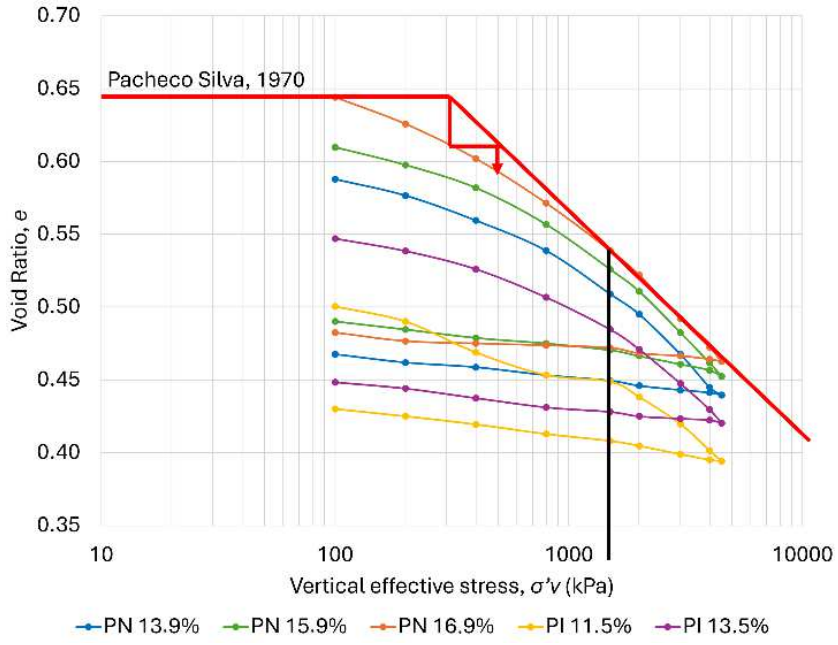
4. RESULTS AND DISCUSSION

4.1. OEDOMETER CONSOLIDATION

Fig. 8 shows the results of the oedometer compaction tests in a single graph. The samples generally presented a precompression stress (σ'_v) of approximately 500 kPa, according to the methodology of Pacheco Silva (1970), but the definitive change in the curve trend to reach the virgin line only occurred at stress levels of 1500 kPa.

All samples followed a similar slope trend for the recompression sections (CS = 0.021), induced by the preconsolidation effect generated by molding, and a similar slope trend for the virgin compression sections – normally consolidated (CC = 0.114) and expansion sections (CE = 0.013). This shows that the CR/CC ratios and CE ranges are consistent with the intervals presented by Terzaghi et al. (1996).

Fig. 8 Results of oedometric tests



In addition, for the sample with the lowest initial void ratio (PI 11.5%), at loading points of 400 kPa (Oed – ID 30) and 800 kPa (Oed – ID 31), there is an indication of a change in the trend of the compression curve slope behavior. This behavior may result in particle evolution due to the breakage of fines and/or the loss of roughness, since the sample has the lowest initial void ratio. However, after continuing the test, for higher loading levels, the slope of the sample was observed in the other tests and followed the same trend.

Importantly, for the tests performed here, the compression and recompression curves for lower initial void ratios flatten so that the initial and final void ratios are closer together. This effect can also be observed in soils, which exhibit less deformation in denser samples.

Evaluating the behavior of the samples as a whole, it was not possible to conclude that there was any convergence of the NCLs for the stress levels tested, a behavior that may be associated with the fabric effect, the organization of the tailings particles, and, consequently, the variation in the values of the geostatic stress ratio, K_0 (σ'_h/σ'_v), the latter characterized by a transitional effect (Altuhafi et al. 2010; Coop and Airey 2003; Ferreira and Bica 2006; Lade and Trads 2014; Nocilla et al. 2006; Rios et al. 2016; Viana da Fonseca et al. 2022; Xu and Coop 2017) that directly influences the tailings compaction process (Rabbi et al. 2018). This condition was also observed in the consolidation stages of the triaxial tests, in which several compression lines were found according to the initial void ratio of the sample.

4.2. TRIAXIAL TESTS, NCL AND CSL

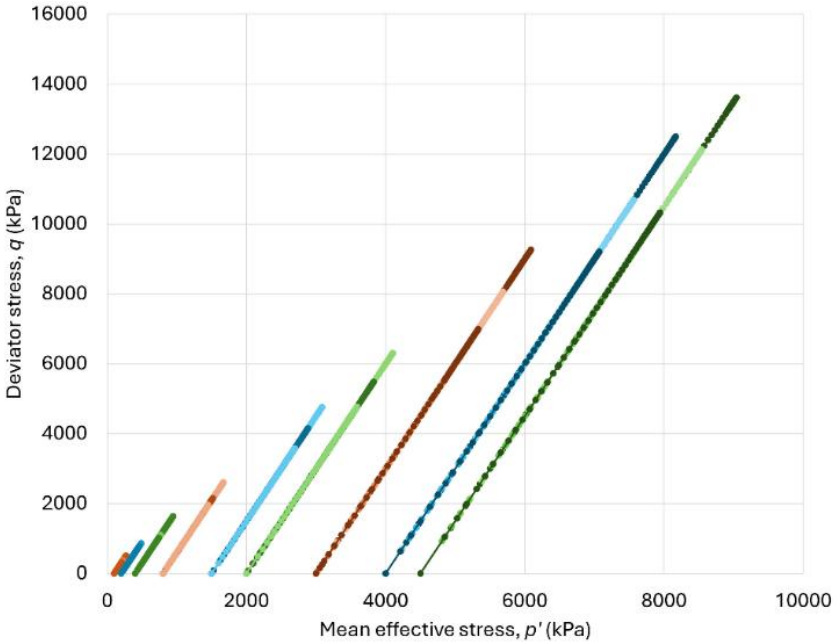
From the triaxial tests, the drained stress trajectories (Fig. 9a) and undrained stress trajectories (Fig. 9b) were obtained. For the drained trajectories, the test endpoints vary, where specimens with a lower initial void ratio, e_0 (after molding) – that is, samples molded with a higher level of compaction effort – presented higher q values (CID – ID 36 and CID – ID 45), as shown in Fig. 10a. This is explained by the fact that the dense samples do not reach the critical state (Jefferies and Been 2016), due to the very clear visualization of several flat shear planes in the experiments and the interpretation of the results for a single element, since these do not align with the same inclination as M_{tc} in the $q - p'$ plane.

Consoli et al. (2024b) have specified that this behavior might be related to a possible change in the CSL to a non-linear behavior of dense samples, due to their materials having a higher level of stiffness, which does not justify hypothetically higher inclination (M_{tc}) in $q - p'$ space.

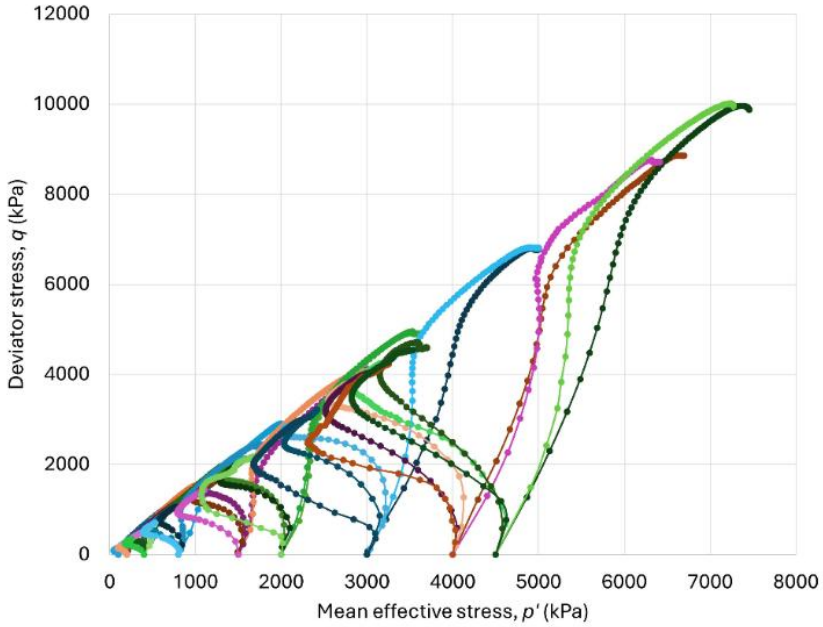
The samples subjected to undrained tests exhibited similar behavior, with samples with lower e_0 values indicating lower excess pore pressure generation during the shear stage (CIU – ID 81 – 4500 kPa and CIU ID – 90 – 4500 kPa) but maintaining alignment in the $q - p'$ plane, as presented in Fig. 10b (Corrêa de Oliveira et al. 2025; Delgado et al. 2023; Silva et al. 2024b). This is again a consequence of the multiple localized shearing surfaces where distinct pore pressures are generated by inflow of water migrating from the preserved homogeneous soil mass to the sliding planes in between. This is indicative

of variations in the contractile and dilating behavior of a sample according to the state parameter (ψ) (Jefferies and Been 2016).

Fig. 9 $q - p'$ plane: (a) CID; (b) CIU

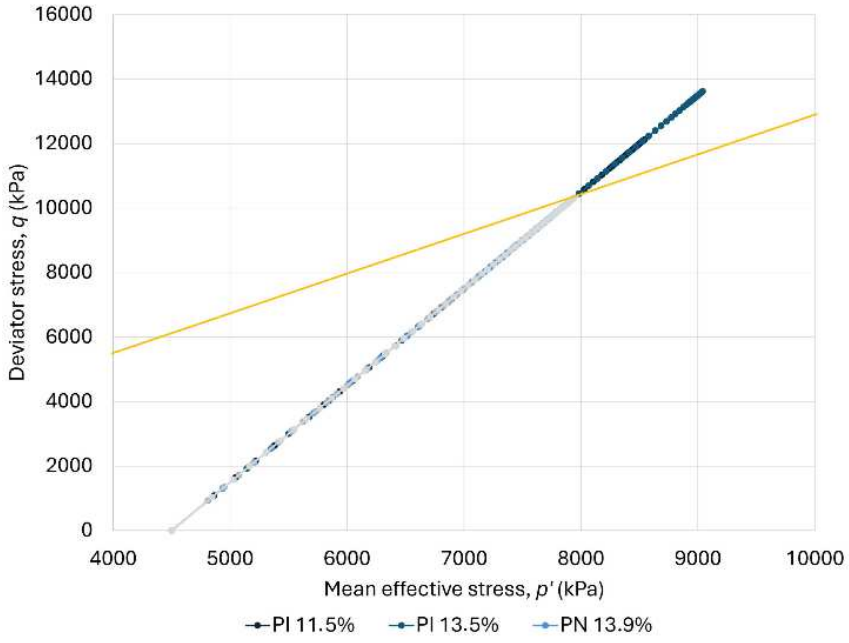


(a)

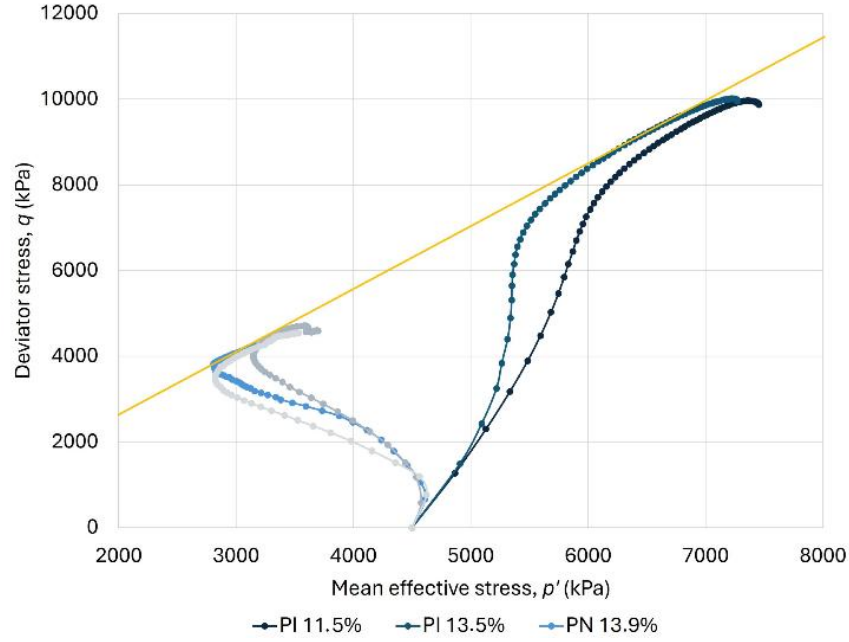


(b)

Fig. 10 Behavior of the $q - p'$ space due to variation in the void ratio: (a) CID of 4500 kPa; (b) CIU of 4500 kPa



(a)

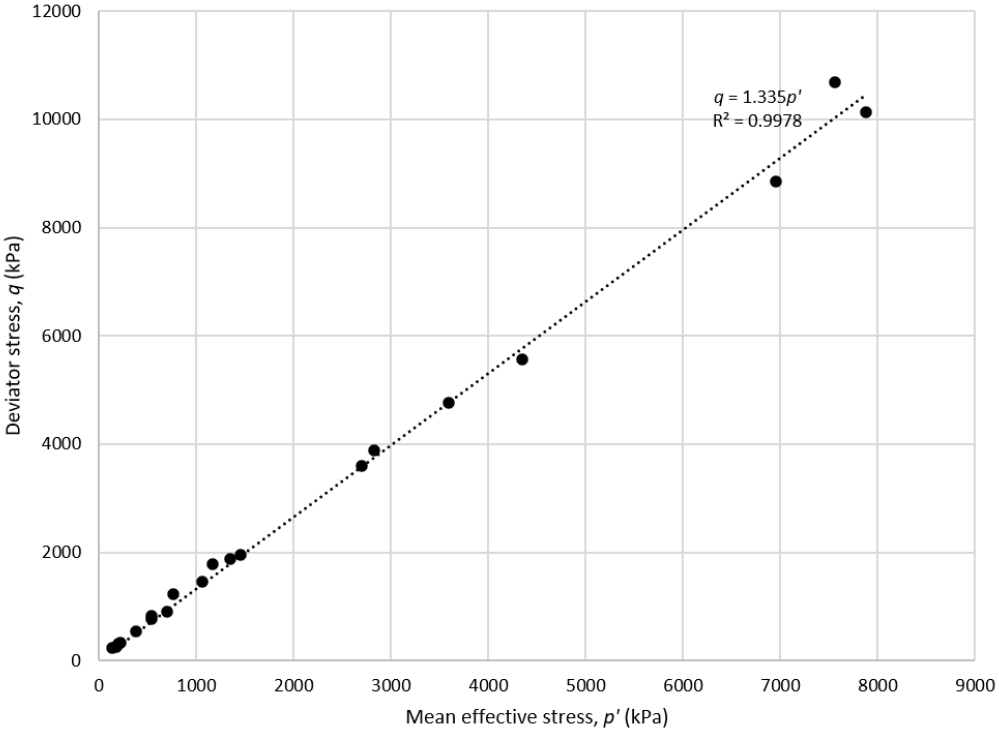


(b)

The sequence of all the tests performed reveals that the average slope (M_{tc}) of the $q - p'$ stress trajectory of the material under study is equal to 1.335 (33.09°), with a high linear approximation (Fig. 11). This shows good adherence to the results. In addition, it is important to mention that this slope is consistent with the results of tests performed on iron ore tailings from

the ‘Quadrilátero Ferrífero’ region, in which there are variations in the value of M_{tc} from 1.250 to 1.470, as shown in Table 7.

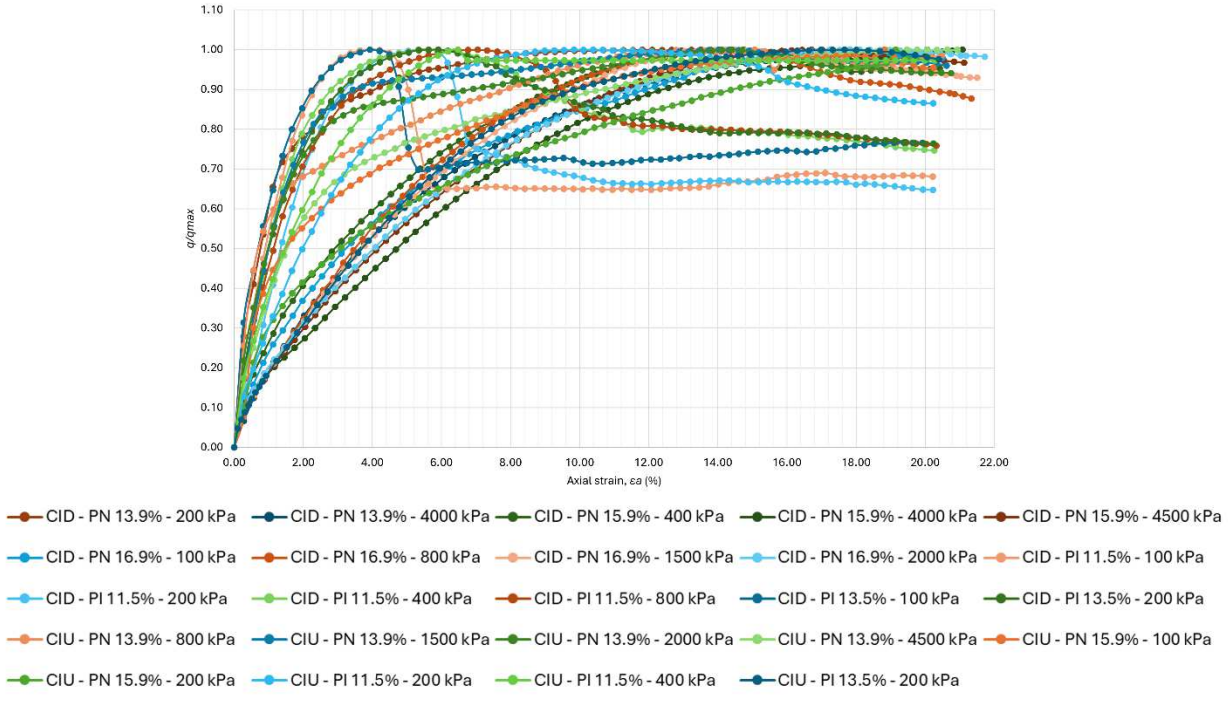
Fig. 11 $q - p'$ plane



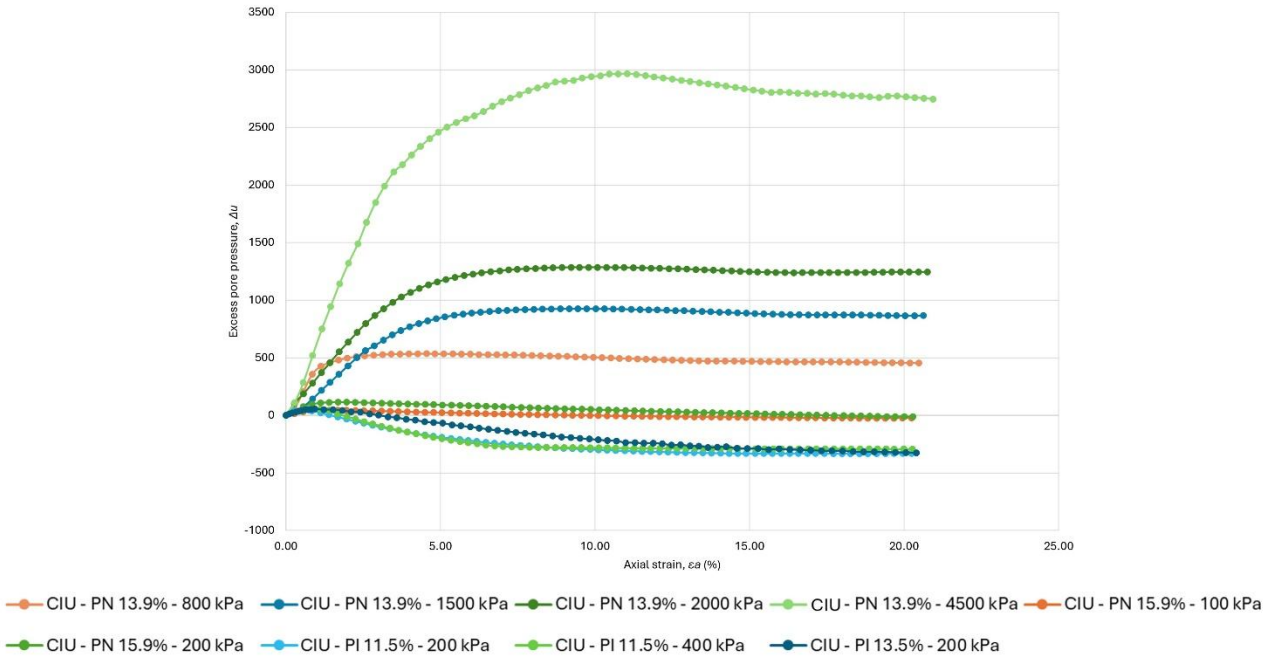
For the tests used to calibrate the CSL parameters in the $e - ln\, p'$ plane and the dilatancy parameters (N_{tc} and χ_{tc}), as shown in Table 6, the relationships between the deviator stress (q) normalized by the maximum deviator stress (q_{max}) and axial strain (εa) are plotted in Fig. 12a for both the CID and CIU tests.

As previously presented, CID tests with peak stress behavior indicate dilatancy conditions in the sample. In addition, no abrupt stress reduction conditions are observed in the CIU samples, i.e., brittleness index (I_{Bu}) values above 0.80 indicate that the samples are nonfragile materials (ICOLD 2025). Fig. 12b shows the verification of the variation in pore pressure (u) versus axial deformation (εa) of CIU tests used in the CSL adjustment.

Fig. 12 (a) Standard deviatoric stress versus axial strain; (b) pore pressure variation versus axial strain



(a)



(b)

353 **Table 7** CSSM parameters for iron ore tailings

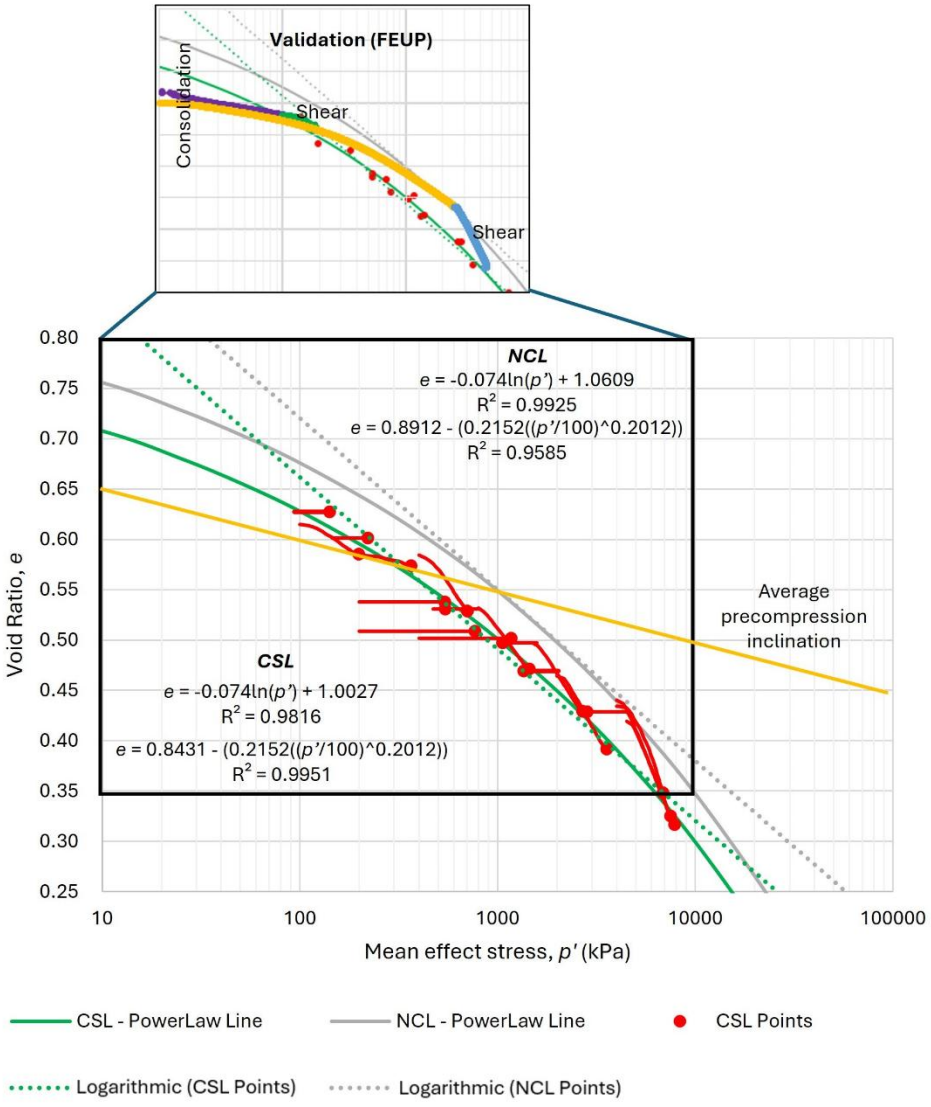
Iron ore tailings	M_{tc}	λ	Γ	a	b	c
This research	1.335	0.074	1.003	0.843	0.215	0.201
Coutinho et al. (2025)	1.340	0.023	0.932	-	-	-
Consoli et al. (2025)	1.370	0.300	1.710	-	-	-
Corrêa de Oliveira et al. (2025)	1.400 – 1.350	-	-	0.770 – 0.860	0.044 – 0.077	0.320 – 0.480
De Andrade et al. (2025)	1.250	-	-	0.730 – 0.920	0.008 – 0.033	0.310 – 1.080
Delgado et al. (2025)	1.366	-	-	1.084	0.031	0.611
Rios et al. (2025)	1.340	-	-	0.866	0.047	0.413
Ccotohuanca et al. (2024)[a]	1.100 – 1.470	0.024 – 0.109	0.870 – 1.430	0.770 – 1.540	0.024 – 0.813	0.060 – 0.770
Consoli et al. (2024a)	1.320 – 1.430	-	-	0.920	0.500	0.170
Consoli et al. (2024b)	1.300 – 1.350	-	-	0.950 – 1.000	0.150	0.232 – 0.245
Faria et al. (2024); Faria (2022); Eloi (2021)	1.397 – 1.449	0.037 – 0.069	1.038 – 1.251	-	-	-
Silva et al. (2024a)	1.340 – 1.490	-	-	0.920	0.500	0.170
Silva et al. (2024b)	1.400	0.060	2.010	1.770	0.080	0.320
Delgado et al. (2023)	1.418	-	-	0.829	0.049	0.401
Santana (2022)	1.350	0.039	0.9903	0.867	0.049	0.452
Viana da Fonseca et al. (2022)	1.360 – 1.420	0.037 – 0.054	1.038 – 1.427	-	-	-
Carneiro 2021; Oliveira (2021)	1.384	0.041	0.800	0.805	0.201	0.150
Reid et al. (2021)[b]	-	0.008 – 0.250	0.621 – 1.300	0.660 – 20.000	0.043 – 19.50	0.007 – 0.720
Robertson et al. (2019)	1.380	-	-	1.230	0.340	0.110
Morgenstern et al. (2016)	1.330	0.024	0.865	-	-	-

354 [a] This study considers the consolidation of various data on the characteristics of tailings; [b] The study considers tests of the
355 same material in several laboratories.

356 Following the completion of tests that maintained good specimen integrity and reached the critical state, the CSL was plotted
357 in the $e - ln\ p'$ plane, as shown in Fig. 13. Both the NCL/CSL semilogarithmic and power-law approximations demonstrated
358 a good fit, as indicated by their R^2 values, above 98% for CSL and above 95% for NCL. The points for which the greatest
359 divergences in behavior occur can be observed at mean effective stress values (p') below 200 kPa and above 6000 kPa, a
360 range close to those of the studies presented by Carneiro (2021); Oliveira (2021) and with behavior similar to the works of
361 Corrêa de Oliveira et al. (2025); Delgado et al. (2023); Delgado et al. (2025); Rios et al. (2025); Santana (2022); Silva et al.
362 (2024a). Thus, it is important to consider the non-linearity of the CSL for structures with high stress levels.

Importantly, the CSL/NCL identified in this study exhibited curvilinear and concave behavior (Fig. 13), unlike studies published by Consoli et al. (2024a); Silva et al. (2024a) (tailings from another mine), which indicated a CSL with convex behavior, which has not been reported in other studies.

Fig. 13 CSL and NCL graphs

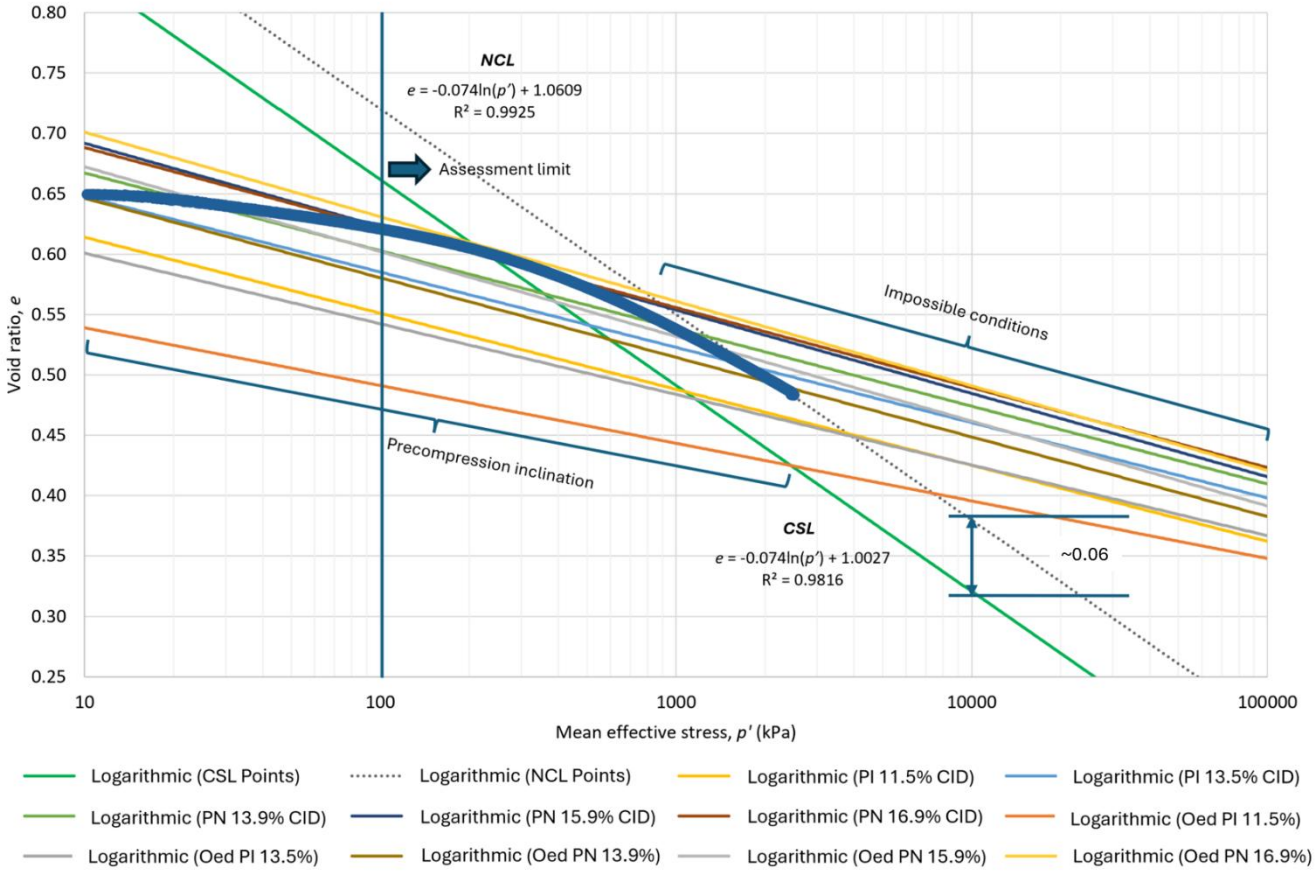


As mentioned earlier, for the execution of oedometric compaction tests (Oed – ID 1 to 45), distinct conditions of precompression and normal consolidation were observed for the samples, in addition to a transitional behavior of the NCL (Ponzoni et al. 2014; Viana da Fonseca et al. 2021), an aspect that can also be identified in the consolidation stage of the triaxial tests. This can be observed at the start of the shearing stage (shear) of the tests, as shown in Fig. 13, which makes it

difficult to define the normal compression line of the tailings. However, to achieve reliable characterization of the NCL, the loosest specimens from the set of tests performed to define this line (Oed – ID 13 to ID 18) were verified. In addition, based on the data from the triaxial tests (CID – ID 91 and ID 92) performed at the FEUP laboratory, it was possible to confirm and verify the similarity of shape of NCL and CSL.

Fig. 14 shows the insertion of all the precompression lines from the oedometric consolidation tests with the average stress corrected by K_0, according to the calculated values of M_{tc} (Carrera et al. 2011; Corrêa de Oliveira et al. 2025; Graham and Jefferies 1986), in addition to the data from the consolidation stages of the triaxial tests. This same graph includes the consolidation phase of the CID – ID 92 test performed at the FEUP laboratory to validate the NCL of the material.

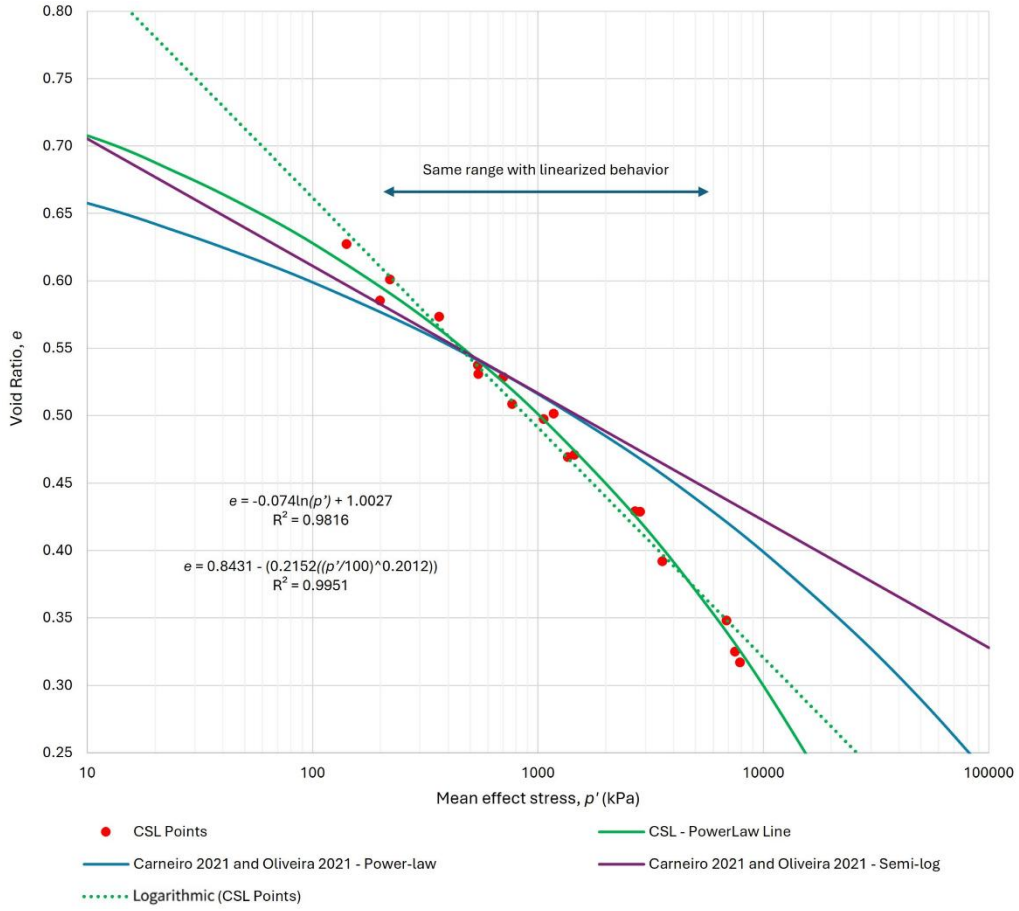
Fig. 14 CSL and NCL of triaxial isotopic compression tests and precompression lines



Based on the results obtained, the maximum state parameter (ψ) is 0.06 and the difference in the linearized range interval of the CSL are lower but are consistent with the results reported by Carneiro (2021); Oliveira (2021) for materials from the same mine. However, compared with those of the other authors, the CSL SemiLog and PowerLaw of the earlier authors

show variations in relation to this study (Fig. 15). This discrepancy can be attributed to the fact that the current tailings have a greater proportion of iron oxides than the tailings evaluated by those authors do, which justifies the increase in the CSL slope (λ) (Torres-Cruz 2019; Torres-Cruz and Santamarina 2020). In addition, there is an increase in the void ratio with p' equal to 1 kPa (Γ), which can also be explained by the reduction in the proportion of fines in the sample (~13% to 16%) (Ji et al. 2024; Wagner et al. 2025). This behavior can also be seen in comparative studies of iron ore tailing samples with variations in their characteristics (amount of iron oxides and proportion of fines), as presented by Viana da Fonseca (2026); Viana da Fonseca et al. (2022) for content of iron oxides of Córrego do Feijão mine where B1 dam failed in 2019.

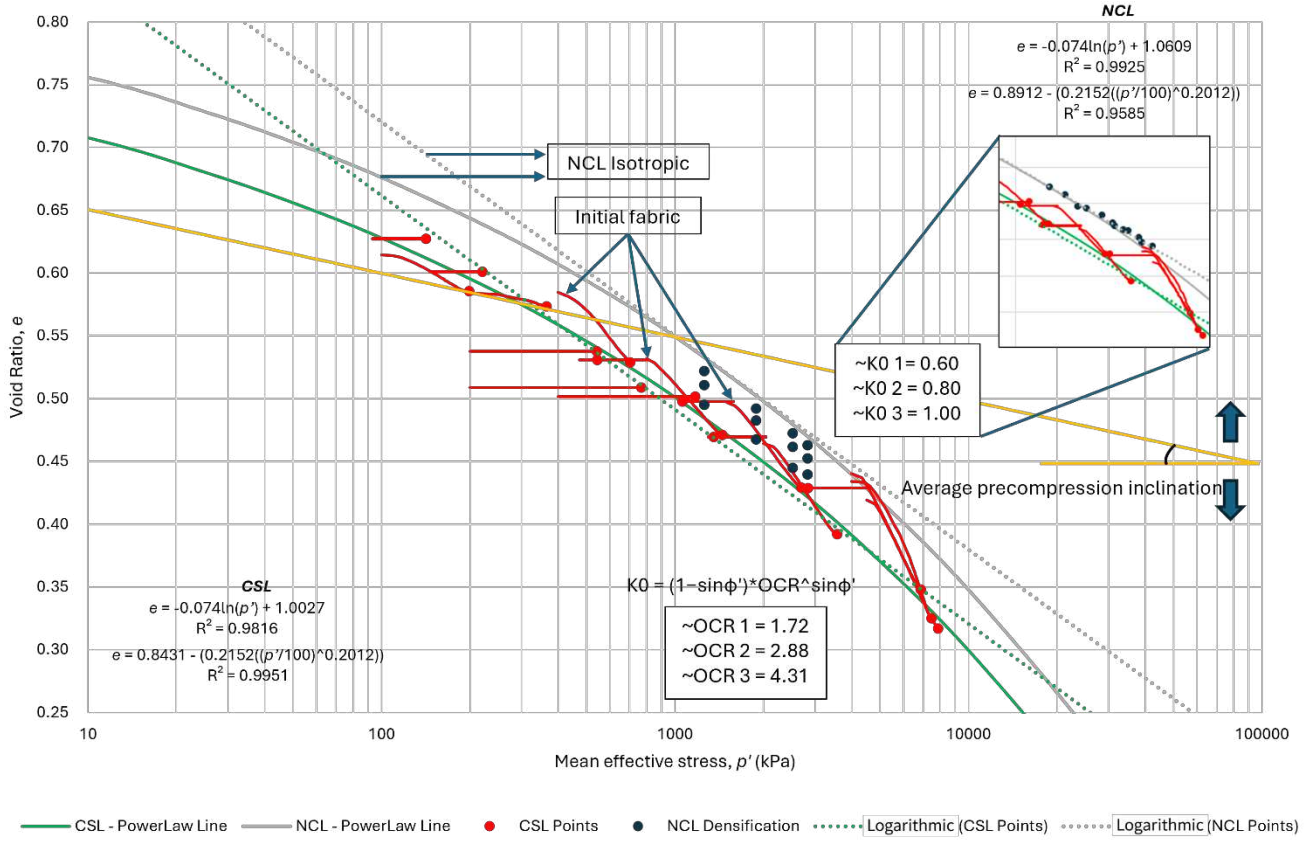
Fig. 15 Comparison with CSL by Carneiro (2021); Oliveira (2021)



As shown in Fig. 16, the ranges of the compaction tests with normally compacted behavior (Oed – ID 7 to 10; Oed – ID 15 to 18; and Oed – ID 24 to 27) were inserted into the CSL graph. The points on the intrinsic consolidation lines (ISLs) were parallel to the NCL and positioned between the CSL and the isotopic normal compression line, similar to studies developed by Delgado et al. (2025). This behavior is typical for NCL, with varying values of K_0 and OCR, due to the influence of the

fabric in the sample formation/molding process (Chu and Wanatowski 2008; Coop 2004; Corrêa de Oliveira et al. 2025; Finno and Rechenmacher 2003; Fourie and Tshabalala 2005; Rabbi et al. 2018; Viana da Fonseca et al. 2022). As shown by the studies mentioned above, this influence is related to the variation in the arrangement of the particles and their interlocking. Considering the behavior of the samples in Fig. 16, the K_0 values were verified so that each of these tests reached the isotropic condition of the NCL. Thus, the compaction tests indicated variations from 0.60 to 1.00 for K_0 and from 1.72 to 4.31 for OCR (Oed – ID 7 to 10, K_0 = 0.60 and OCR = 1.72; Oed – ID 15 to 18, K_0 = 0.80 and OCR = 2.68; and Oed – ID 24 to 27, K_0 = 1.00 and OCR = 4.31).

Fig. 16 Influence of K_0 from compaction tests in relation to NCL

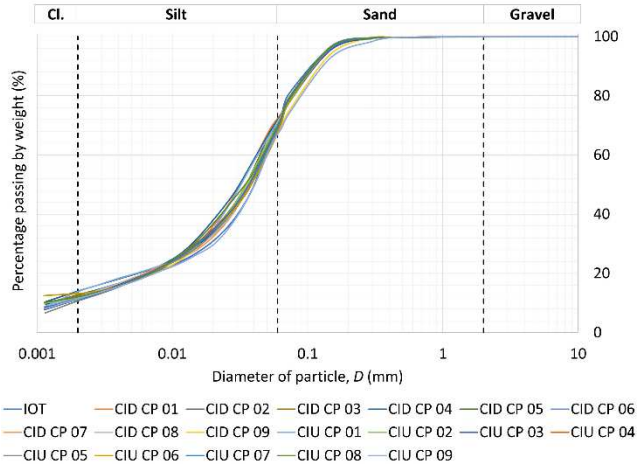


For the parameters obtained for the slope of the stress path line (M_{tc}) and for the critical state line, both for SemiLog (Γ and λ) and for PowerLaw (a, b, and c), as shown in Table 7, the values obtained are consistent with recent research involving iron ore tailings from mines in the 'Quadrilátero Ferrífero' region, see Viana da Fonseca et al. (2022); Carneiro (2021); Oliveira (2021).

4.3. PARTICLE SIZE DISTRIBUTION AFTER TRIAXIAL TESTS

To evaluate the cause of the change in the CSL trend (non-linear), particle size distribution tests were performed on all the triaxial test samples after the shearing stage. The average results of the CID and CIU triaxial tests are shown in Fig. 17 (numbered from 1 to 9, in ascending order according to the level of consolidation stress). As seen, in macro terms, the changes are not significant in terms of particle size. This is consistent with the results obtained by Corrêa de Oliveira et al. (2025).

Fig. 17 Average particle size distribution after testing



After performing these tests, the particle breakage index (B_g) proposed by Marsal (1967) [Eq. (9)] was evaluated in relation to the initial (p_{ij}) and final (p_{fj}) particles sizes.

$$B_g = \Sigma_{(i=1)}^{n} |\Delta p_{ij} - \Delta p_{fj}| \quad \text{(Eq. 9)}$$

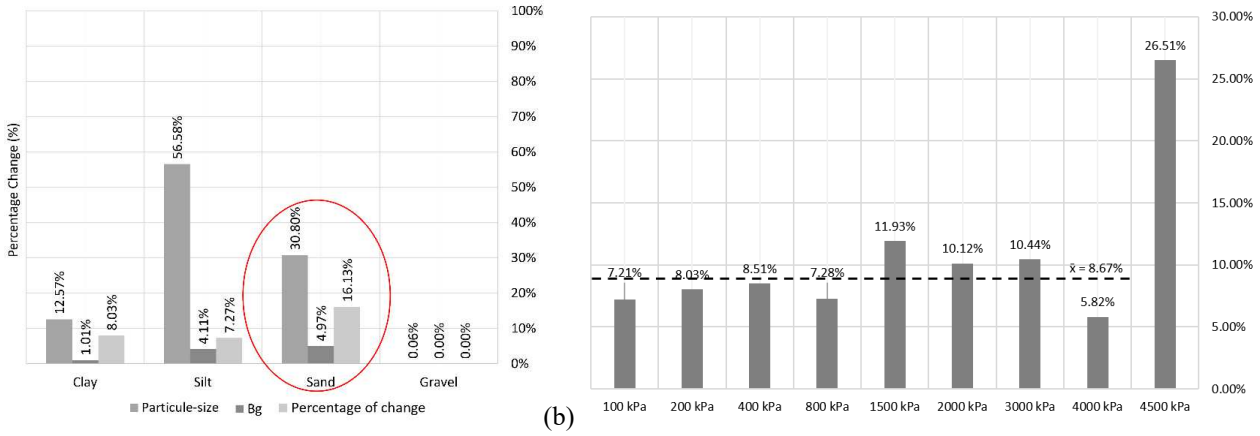
Based on this assessment, the average particle breakage is mainly related to the sandy fraction (Fig. 18a). This breakage is justified by the rigid behavior but low ductility of SiO_2, which is due to stronger multidirectional covalent atomic bonds (high effort) than those of Fe_2O_3, which exhibits ductile behavior and greater deformation without particle breakage, which is justified by fewer directional ionic bonds (lower effort) (Chicot et al. 2011).

Fig. 18b shows the evolution of the B_g value based on each compaction stress level of the tests. The values presented are the average of the tests shown in Fig. 17.

As can be seen, and consistent with the findings regarding the curvature of the CSL, only the σ'_v tests at 4500 kPa exhibit a particle breakage of approximately 26.51%. These are precisely the tests that exhibit p' values $>$ 6000 kPa during the shear stage, indicating a tendency for the CSL to change. The remaining tests, for lower stress levels, show a certain degree of homogeneity, with averages close to 8.67%.

During the imaging tests (SEM) on the post triaxial test material, no morphological changes in the tailing grains were found. However, as the B_g index of the sandy fraction was high, the IOT sample was separated, and a segregated evaluation of the scanning electron microscope image was performed for this fraction. In this evaluation (Figs. 19b and 19c), a higher frequency of smaller sand grains was found, revealing morphological changes in this part of the tailings (compared with the samples prior to the triaxial tests). This may explain the change in the CSL trend, as presented by Carvalho et al. (2024); Cho et al. (2006); Delgado et al. (2023); Lashkari et al. (2020); Rios et al. (2025); Viana da Fonseca et al. (2022); Yang et al. (2019).

Fig. 18 Grain breakage index: (a) average breakage by grain size; (b) average breakage by stress level



(a) (b)

Due to the granulometric and morphological changes observed in the sample at average effective stresses above 6000 kPa, this study proposes a new division of the $e - ln\, p'$ plane, as suggested by Carrera et al. (2011) for high stress levels or strain-hardening behavior ranges. This illustrates how this behavior is divided into strain hardening and fabric changes (Fig. 19a), indicating that, after the loading stages involving undrained strain-hardening behavior, the samples begin to exhibit particle breakage and/or morphological changes in the grains. The evolution of CSL in soils is associated with variations in grain size distribution and mineralogical structure of the materials.

Fig. 19 (a) Division of CSL areas (adapted from Carrera et al. 2011); (b) Scanning electron microscopy (SEM) – initial; (c) Scanning electron microscopy (SEM) – particles size and morphology evolution – sand particle breakage

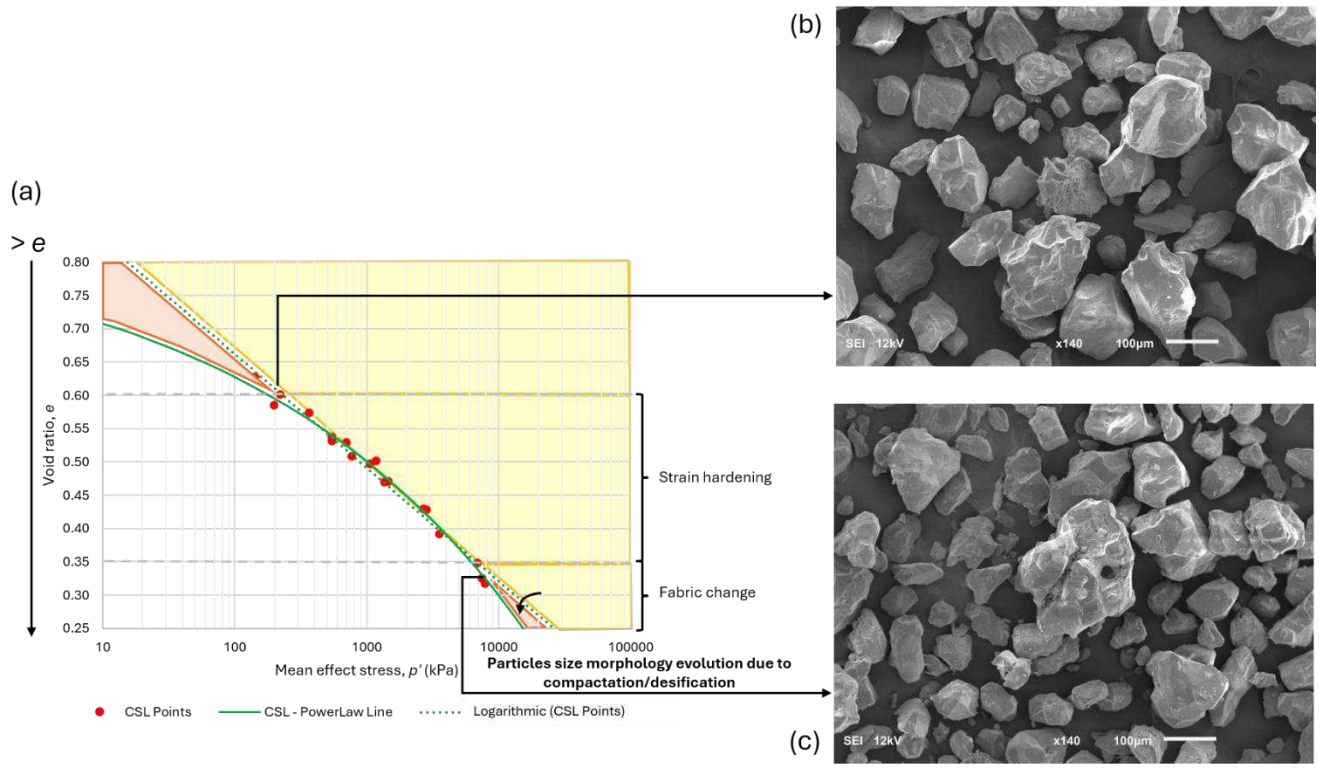
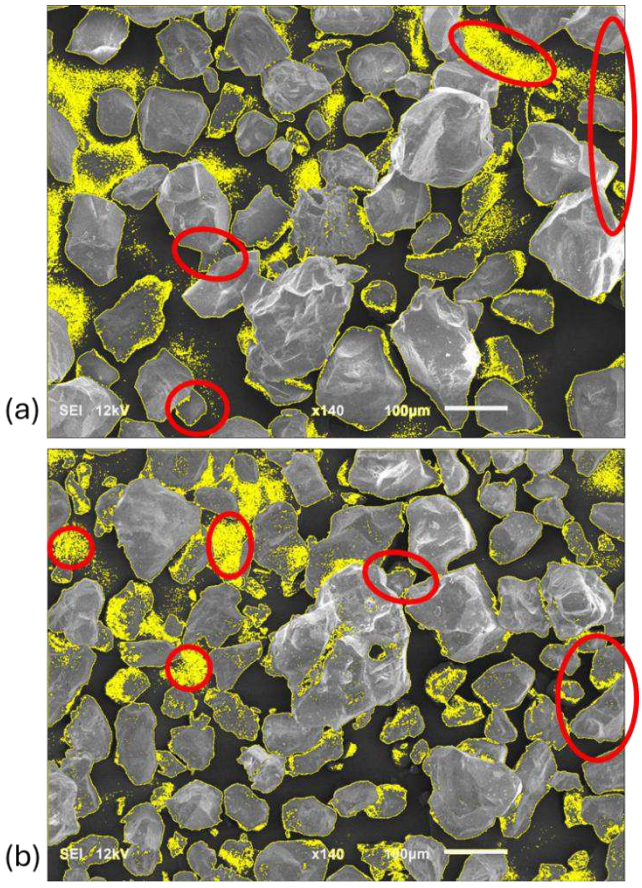


Fig. 19b and Fig. 19c were analyzed using ImageJ software to measure the average particle area, circularity, aspect ratio, and angularity. To perform these measurements, only particles that were fully exposed and had sufficient definition for the measurements were extracted from the SEM images. In other words, particles embedded in tangles and present at the edges of the images were discarded, as shown in Fig. 20.

This analysis aimed to identify changes in the sandy fraction of the tailings resulting from high-stress tests. A change in the physical characteristics of the material was observed, with a reduction in area and angularity and an increase in circularity and aspect ratio (Table 8). Thus, it is concluded that these morphological changes indicate a reduction in the size of the tailings grains and an increase in their sphericity. This evaluation is similar to the studies conducted by John et al. (2023).

458 **Fig. 20** Image interpretation to assess changes in tailings particles and highlighting discarded areas and particles: (a)
459 Scanning electron microscopy (SEM) – initial; (b) Scanning electron microscopy (SEM) – particles size and morphology
460 evolution – sand particle breakage



461

462 **Table 8** Changes in tailings particle morphology following high-stress testing

Parameter	Initial	Particles size and morphology evolution
Mean area (µm²)	4180	3420
Angularity	0.750	0.640
Circularity	0.660	0.710
Aspect Ratio	1.550	1.420

463

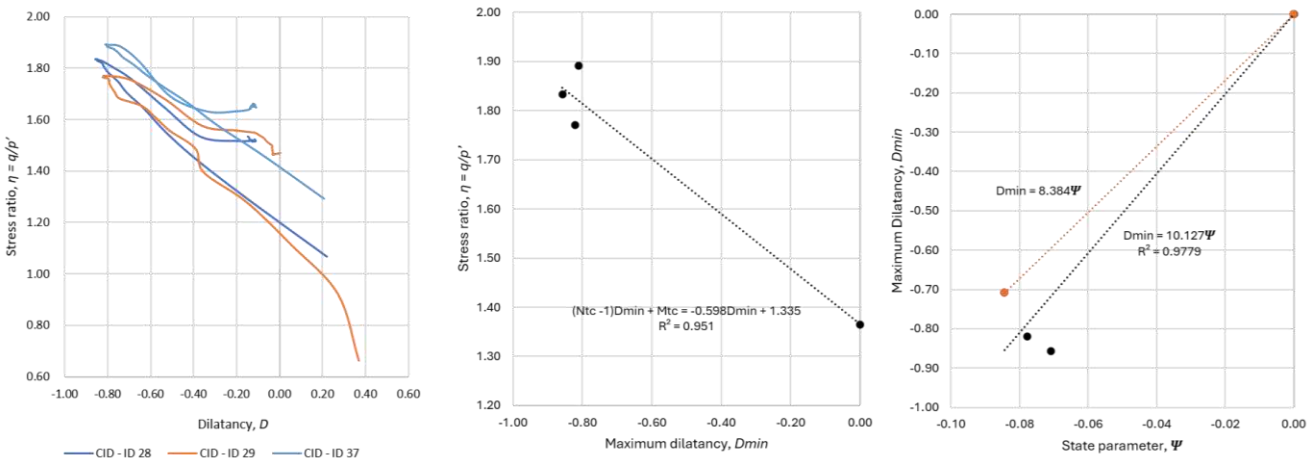
4.4. DILATANCY

To evaluate the dilatancy conditions of the IOT under study, dense samples from drained triaxial tests were used. The selected specimens were pre-compacted with high compressive stress levels, lower void ratios/higher molding effort and exhibited more pronounced dilatancy behavior (CID – ID 28, CID – ID 29 and CID – ID 37). Next, in Fig. 21a, 21b, and 21c, the stress ratios (η) in relation to the dilatancy (D_{min}) of the samples are represented. Eq. (10) and Eq. (11) show the formulations used to define the parameters of the dilatancy coefficient (χ_{tc}) and the volumetric coupling parameter of dilatancy (N_{tc}).

$$\eta = M_{tc} - (1 - N_{tc})\, x\, D_{min} \quad \text{(Eq. 10)}$$

$$D_{min} = \chi_{tc}\, x\, \psi \quad \text{(Eq. 11)}$$

Fig. 21 Dilatancy relations: (a) $\eta - D$; (b) $\eta - D_{min}$; (c) $D_{min} - \psi$



Thus, the results obtained for N_{tc} and χ_{tc} are 0.402 and 8.384, respectively. For the χ_{tc} value, it is important to mention that the result obtained for sample CID – ID 37 was used as a reference because of its better test performance.

As shown in Table 9, the value of N_{tc} is consistent with other studies (Eloi 2021; Faria 2022; Faria et al. 2024; Morgenstern et al. 2016). With respect to the value obtained for χ_{tc}, a higher index than those identified in the literature are observed, but the result is consistent with studies developed by Carneiro (2021); Oliveira (2021) for tailings from the same mine.

480 **Table 9** Dilatancy and stiffness parameters of iron ore tailings

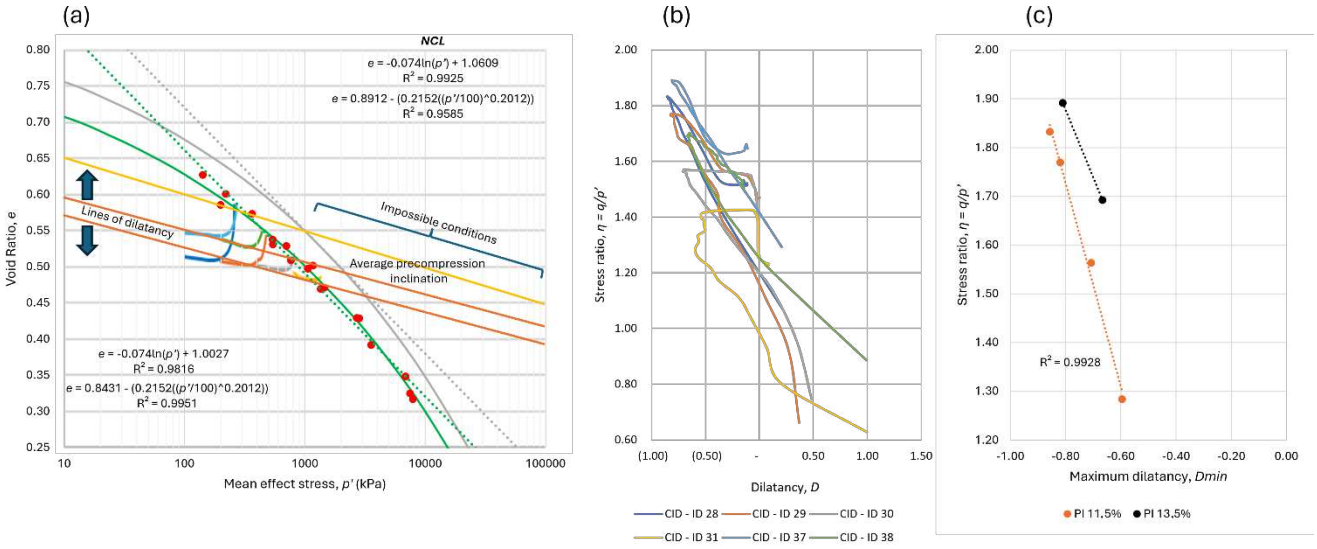
Iron ore tailings	N_{tc}	χ_{tc}	G_{ref}	m
This research	0.402	8.384	34.614	0.478
Coutinho et al. (2025)	0.310	4.000	60.000	0.450
Consoli et al. (2025)	0.350	0.750	32.700	0.860
Delgado et al. (2025)	0.841	3.410	-	-
Rios et al. (2025)	0.360	3.000	28.810	0.630
Consoli et al. (2024b)	0.210 – 0.230	-	2.90 – 12.50	0.550
Faria et al. (2024); Faria (2022); Eloi (2021)	0.498	5.822	50.000	0.500
Santana (2022)	0.580	6.200	53.000	0.595
Silva et al. (2024b)	0.300	4.880	-	-
Carneiro (2021); Oliveira (2021)	0.006	8.160	18.000 – 50.000	0.300 – 0.580
Robertson et al. (2019)	0.270	6.000	100.000	0.500
Morgenstern et al. (2016)	0.380	7.300	60.000	0.450

481

482 Significantly, during the interpretation of the tests for the calibration of the N_{tc} and χ_{tc} parameters, the dilatancy behavior
483 of the material presented variations in η according to the molding effort of the sample and, consequently, by the material
484 fabric. This behavior was also identified in studies by Gunnteg et al. (2025); Reid et al. (2025); Shuttle and Jefferies (2005)
485 and was justified in these works by the moist tamping molding method not being ideal for the calibration of these parameters.
486 However, this condition may be associated with the existence of various dilatant state lines (DSLs) of the IOT, each of which
487 influences the behavior of these parameters.

488 Fig. 22a presents the various parallel dilatancy lines (DSLs), which can also be identified as the predensification lines of the
489 sample. Figs. 22b and 22c indicate that these lines generate linearized behaviors with similar slopes for the D and D_{min}
490 versus η relationships. However, as shown in Fig. 22c, for each initial void ratio (e_i), there is a translation of this alignment
491 on the η axis. Compared with the denser samples, the less dense samples are positioned with higher stress ratios. This
492 condition indicates that N_{tc} and χ_{tc}, like the $G_0 - p'$ relationship, also depend on the condition of the sample and are not
493 purely intrinsic characteristics of the material.

Fig. 22 Interpretation of the dilatancy relations: (a) $\eta - D$; (b) $\eta - D_{min}$; (c) $D_{min} - \psi$



It should be emphasized that the parameters χ_{tc} and N_{tc} were calculated based on the type of remolding and the fabric of the samples in this study; however, it is important to note that these results may vary depending on changes to these samples. In other words, these parameters are not intrinsic to the IOT.

4.5. S-CPTU TESTS

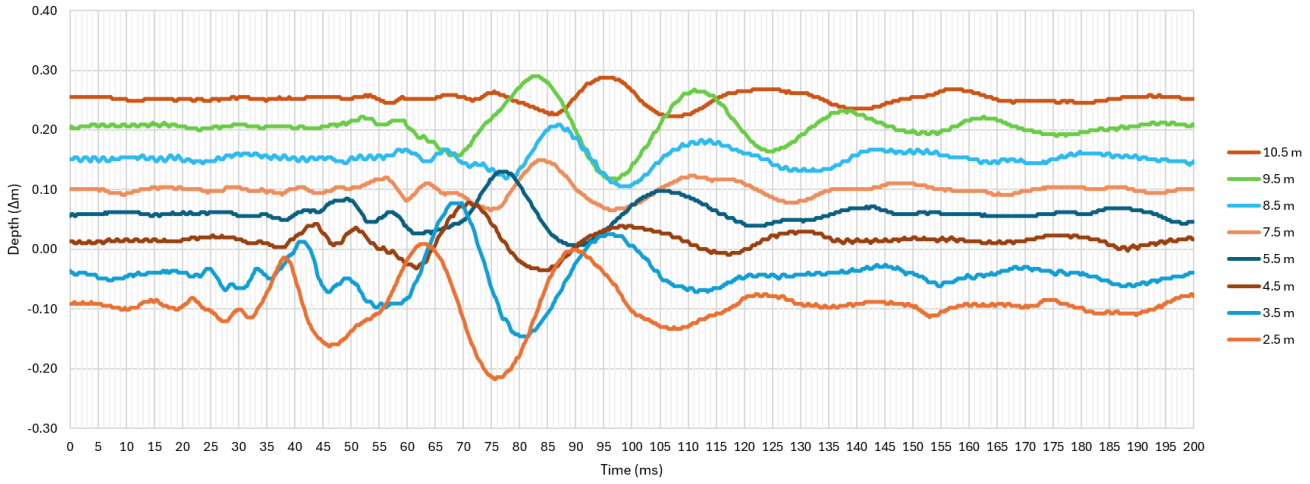
For the calibration of the shear modulus (G_0) versus average effective stress (p'), seismic tests were performed during the execution of a CPTu in an experimental dry stack (Fig. 7). The compaction conditions were similar to those used for molding samples CID – ID 1 to 9 and CIU – ID 46 to 54, but with the actual influence of K_0 from dry stacking. Thus, tests were performed at depths of 2.5 m to 11.5 m (Fig. 23), where the existence of a water level was observed. From these tests, the shear wave propagation velocity (V_s) associated with the test depth and propagation time was determined. With this, the value of G_0 was calculated via Eq. (12).

$$G_0 = \gamma \, x \, V_s^{\,2} \qquad \text{(Eq. 12)}$$

The G_0 calculations were performed based on the interval velocities from each seismic test. Due to the height of the experimental embankment, the maximum value of p' reached was 54 kPa. The specific weight of the material ranged from 19.72 kN/m³ to 21.28 kN/m³. These two values (p' and γ) were calculated for each elevation of the test, based on correlations

with the data measured in the S-CPTu test. The value of K_0 used was 0.455, based on the value of M_{tc} found in the triaxial tests and the Jaky (1944) correlation. The water table was identified at 1.5 m from the initial test elevation. The value of G_0 was extrapolated to 100 kPa (p_{ref}).

Fig. 23 Calibration of G_0 via S-CPTu tests (shear waves)

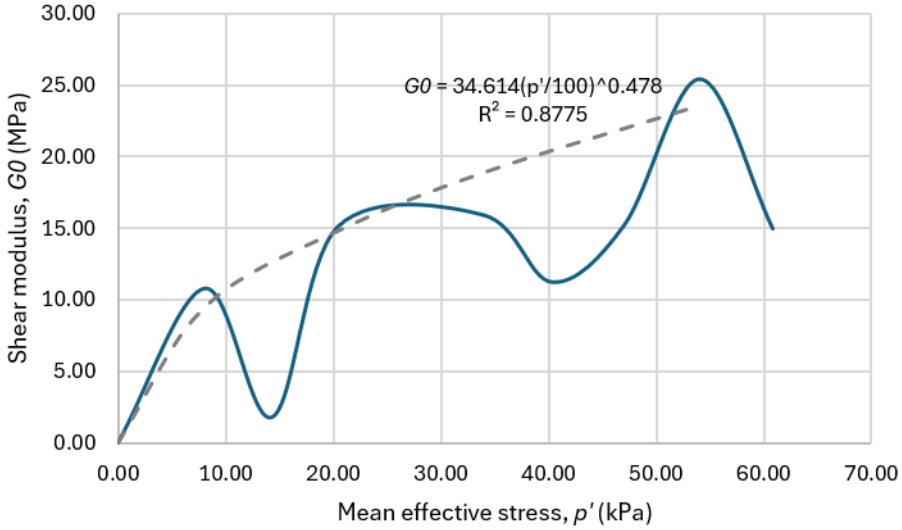


Even with the limitations of the S-CPTu test range, the G_0 values obtained for each S curve were verified in relation to the p' stress measurement corresponding to each test elevation. With this, the relationship between the parameters was constructed according to Eq. (13) and is shown on Fig. 24. The correlation $G_0 - p'$ was estimated based on the data points with the highest consistency of measurements.

Other tailings studied in the 'Quadrilátero Ferrífero' region, evaluated using bender elements (Table 9), present significant variations in the parameters G_{ref} and m. In this study, which uses field seismic tests, these values are 34.614 MPa and 0.478, respectively, similar to the results obtained by Carneiro (2021); Consoli et al. (2025); Oliveira (2021); Rios et al. (2025) for iron ore tailings.

$$G_0 = G_{ref}\ x\ (p' / p_{ref})^m \qquad \text{(Eq. 13)}$$

525 **Fig. 24** $G_0 - p'$ ratio



526

527

528 **4.6. GEOMECHANICAL PARAMETERS**

529 Finally, the consolidation of all the IOT parameters calculated in this study is presented in Table 10. These values, as shown
530 throughout the article, are consistent with the variations reported in the literature, although they exhibit distinctive
531 characteristics.

532 **Table 10** Characteristics of the IOT researched

Characteristic parameters of the NorSand constitutive model		
Properties of the critical state	M_{tc}	1.335
	N_{tc}	0.402
	χ_{tc}	8.384
	λ	0.074
	Γ	1.003
	a	0.843
	b	0.215
	c	0.201
Elastic modules	G_{ref}	34.614
	m	0.478

5. CONCLUSIONS

First, it is important to note the need to conduct tests on tailings using detailed methodologies to accurately determine the geomechanical parameters of the material.

Furthermore, based on the set of tests performed, the iron ore tailings under study exhibit a remarkably non-linear CSL, especially at high effective mean stresses (above 6000 kPa). Morphological changes and even particle breakage were observed in the coarse-grained fraction of the tailings (sandy fraction), which was composed of silica. This explains the change in the CSL/NCL behavior of the material.

In addition, the amount of fines and iron oxides can directly impact the critical state line and normal compression line parameters, where a greater amount of iron indicates an increase in the CSL slope and an increase in the amount of fines results in a reduction in the void ratio at the average effective stress of 1 kPa.

The fabric effect was also observed in the samples, with the K_0 and OCR parameters varying according to the initial void ratios of the oedometric consolidation tests. Thus, the transitional effect was verified in the normal consolidation stress ranges of these tests.

The parameters calculated for the $G_0 - p'$ relationship, obtained by performing an S-CPTu test, were also consistent with results reported in the literature.

Finally, the conclusions obtained in this research reinforce the importance of developing studies and computational models of tailings storage facilities (TSFs) with constitutive models that address the CSSM and the non-linearity of the CSL. Oversimplifying the SemiLog representation of the critical state line may lead to misinterpretations of the geomechanical behavior of tailings disposal structures of great height subjected to high stresses.

6. ACKNOWLEDGEMENTS

The authors would like to thank the Federal University of Viçosa (UFV) and the Faculty of Engineering of the University of Porto (FEUP) for their technical support in conducting this study. Financial support for the experimental program was provided through a project coordinated by Professor Eduardo Marques at the Viçosa Foundation for Art, Culture, and Education for Citizenship (FACEV), a supporting foundation of UFV and Brazilian National Research Council (CNPq)

Project No. 311221/2023-8. The activities carried out at FEUP were jointly funded by FACEV and project UID/4708/2025 of CONSTRUCT – Institute of Research and Development in Structures and Construction, coordinated by António Viana da Fonseca. The authors also acknowledge the financial support provided by the Coordination for the Improvement of Higher Education Personnel (CAPES).

7. STATEMENTS AND DECLARATIONS

7.1. COMPETING INTERESTS

The authors declare that they have no known competing financial interests or personal relationships that could have appeared to influence the work reported in this paper.

7.2. AUTHOR CONTRIBUTIONS

Conceptualization: Leonardo da Silva Machado, Eduardo Antonio Gomes Marques, António Viana da Fonseca, Bruno Guimarães Delgado;

Methodology: Leonardo da Silva Machado, Eduardo Antonio Gomes Marques, António Viana da Fonseca, Bruno Guimarães Delgado;

Formal analysis and investigation: Leonardo da Silva Machado, Eduardo Antonio Gomes Marques, António Viana da Fonseca;

Writing – original draft preparation: Leonardo da Silva Machado;

Writing – review and editing: Leonardo da Silva Machado, Eduardo Antonio Gomes Marques, António Viana da Fonseca, Bruno Guimarães Delgado, Roberto Lopes Ferraz;

Funding acquisition: Eduardo Antonio Gomes Marques, António Viana da Fonseca;

Resources: Eduardo Antonio Gomes Marques, António Viana da Fonseca; and

Supervision: Eduardo Antonio Gomes Marques, António Viana da Fonseca, Bruno Guimarães Delgado, Roberto Lopes Ferraz.

All authors read and approved of the final manuscript.

7.3. DATA AVAILABILITY STATEMENT

The data supporting the findings of this study are available upon reasonable request to the corresponding author, Leonardo da Silva Machado, via email at leonardo.d.machado@ufv.br.

8. NOTATION

List of symbols:

AASHTO – American Association of State Highways and Transportation Officials

ASTM – American Society for Testing and Materials

εa – Axial strain

B_g – Breakage index

I_{Bu} – Brittleness index (undrained)

Cc – Coefficient of curvature

Cu – Coefficient of uniformity

CC – Compression index

λ – Compression index in SemiLog/Logarithm CSL

CPTu – Cone penetration test with pore pressure measurement

CAPES – Coordenação de Aperfeiçoamento de Pessoal de Nível Superior

CSSM – Critical state soil mechanics

CSL – Critical state line

603 Chr – Chromite

604 Sr – Degree of saturation

605 q – Deviator stress

606 εq – Deviatoric strain

607 $Diam$ – Diameter

608 D – Dilatancy

609 χ_{tc} or χ – Dilatancy coefficient

610 DSL – Dilatant state line

611 σ'_c – Effective consolidation stress

612 σ'_h – Effective horizontal stress

613 σ'_v – Effective vertical stress

614 EDS – Energy dispersive X-ray spectroscopy

615 CE – Expansion index

616 m – Exponent for the stress dependency of the shear modulus

617 FEUP – Faculdade de Engenharia da Universidade do Porto

618 p_{fj} – Final diameter of each sieve

619 FACEV – Fundação Artística, Cultural e de Educação para a Cidadania de Viçosa

620 p_{ij} – Initial diameter of each sieve

621 ISL – Intrinsic consolidation line

622 e_i – Initial void ratio (after consolidation in the triaxial compression test)

623 e_0 – Initial void ratio (after moist tamping)

IOT – Iron ore tailing

Gt – Goethite

K_0 – Coefficient of earth pressure at rest

H – Height

Hm – Hematite

w – Humidity

LVDT – Linear Variable Differential Transformer

Mt – Magnetite

q_{max} – Maximum deviator stress

D_{min} – Maximum dilatancy

γ_d – Maximum dry unit weight

e_{max} – Maximum void ratio

p' – Mean effective stress

D_{50} – Median particle diameter

e_{min} – Minimum void ratio

a – Model parameter in the PowerLaw CSL

b – Model parameter in the PowerLaw CSL

c – Model parameter in the powerLaw CSL

NCL – Normal compression line

Oed – Oedometer test

Wot – Optimal humidity

645 OCR – Overconsolidation ratio

646 u – Pore pressure

647 PDA – Potential damage associated

648 PI – Proctor with altered effort (intermediate)

649 PN – Proctor with normal effort

650 B – Skempton's pore pressure parameter B

651 Qz – Quartz

652 G_{ref} – Reference shear modulus

653 p_{ref} – Reference mean stress

654 SEM – Scanning electron microscope

655 S-CPTu – Seismic piezocone penetration test with pore pressure measurement

656 V_s – Shear wave velocity

657 G_0 – Small-strain shear modulus

658 G_s – Specific gravity of solids

659 ψ – State parameter

660 M_{tc} – Stress ratio at the critical state

661 η – Stress ratio (q/p')

662 CS – Swelling index

663 TSF – Tailings storage facility

664 CID – Triaxial consolidated isotropically drained

665 CIU – Triaxial consolidated isotropically undrained

666 USCS – Unified Soil Classification System

667 γ – Unit weight

668 UFV – Universidade Federal de Viçosa

669 e – Void ratio

670 e_{CSL} – Void ratio at the critical state line

671 Γ – Void ratio with p' at 1 kPa in SemiLog/Logarithm CSL

672 N_{tc} or N – Volumetric coupling parameter, dilatancy slope

673 εv – Volumetric strain

674 XRF – X-ray Fluorescence

675 S – Wave s

676

677 **9. REFERENCES**

678 AASHTO (2017a) Moisture–density relations of soils using a 2.5-kg rammer and a 305-mm drop (standard Proctor
679 method) (AASHTO T99-17). American Association of State Highway and Transportation Officials, Washington, DC

680 AASHTO (2017b) Moisture–density relations of soils using a 4.5-kg rammer and a 457-mm drop (modified Proctor
681 method) (AASHTO T180-17). American Association of State Highway and Transportation Officials, Washington, DC

682 Altuhafi F, Baudet BA, Sammonds P (2010) The mechanics of subglacial sediment: an example of new transitional
683 behaviour. Can Geotech J 47:775–790. https://doi.org/10.1139/T09-136

684 Amoah N, Dressel W, Fourie AB (2018) Characterisation of unsaturated geotechnical properties of filtered magnetite
685 tailings in a dry stack facility. In: Jewell RJ, Fourie AB (eds) Paste 2018: Proceedings of the 21st International Seminar
686 on Paste and Thickened Tailings. Australian Centre for Geomechanics, Perth, pp 375–388.
687 https://doi.org/10.36487/ACG_rep/1805_31_Amoah

688 ANM (2025) Resolution No. 220/2025. Diário Oficial da União, Brasília

689 Arroyo M, Gens A (2021) Computational analyses of Dam I failure at the Córrego do Feijão mine in Brumadinho.
690 Technical report, CIMNE, Barcelona

691 Assis Júnior FE (2026) O estudo do efeito de trajetórias de direção não é convencional na modelagem do comportamento
692 de grandes estruturas de aterros. Dissertação de mestrado, Faculdade de Engenharia, Universidade do Porto, Porto,
693 Portugal

694 ASTM (2016a) Standard test methods for maximum index density and unit weight of soils using a vibratory table
695 (ASTM D4253-16). ASTM International, West Conshohocken, PA

696 ASTM (2016b) Standard test methods for minimum index density and unit weight of soils and calculation of relative
697 density (ASTM D4254-16). ASTM International, West Conshohocken, PA

698 ASTM (2017) Standard practice for classification of soils for engineering purposes (Unified Soil Classification System)
699 (ASTM D2487-17). ASTM International, West Conshohocken, PA. https://doi.org/10.1520/D2487-17

700 ASTM (2020a) Standard test method for consolidated undrained triaxial compression test for cohesive soils (ASTM
701 D4767-11(2020)). ASTM International, West Conshohocken, PA. https://doi.org/10.1520/D4767-11

702 ASTM (2020b) Standard test method for electronic friction cone and piezocone penetration testing of soils (ASTM
703 D5778-20). ASTM International, West Conshohocken, PA. https://doi.org/10.1520/D5778-20

704 ASTM (2020c) Standard test method for consolidated drained triaxial compression test for soils (ASTM D7181-20).
705 ASTM International, West Conshohocken, PA. https://doi.org/10.1520/D7181-20

706 ASTM (2021) Standard test methods for laboratory compaction characteristics of soil using standard effort (12,400 ft-
707 lbf/ft³ (600 kN-m/m³)) (ASTM D698-12(2021)). ASTM International, West Conshohocken, PA.
708 https://doi.org/10.1520/D0698-12R21

709 ASTM (2021a) Standard test methods for laboratory compaction characteristics of soil using modified effort (56,000 ft-
710 lbf/ft³ (2,700 kN-m/m³)) (ASTM D1557-12(2021)). ASTM International, West Conshohocken, PA.

711 ASTM (2021b) Standard test method for particle-size distribution (gradation) of fine-grained soils using the
712 sedimentation (hydrometer) analysis (ASTM D7928-21E01). ASTM International, West Conshohocken, PA.
713 https://doi.org/10.1520/D7928-21E01

714 ASTM (2023) Standard test methods for specific gravity of soil solids by the water displacement method (ASTM D854-
715 23). ASTM International, West Conshohocken, PA. https://doi.org/10.1520/D0854-23

716 ASTM (2025a) Standard test methods for one-dimensional consolidation properties of soils using incremental loading
717 (ASTM D2435/D2435M-25). ASTM International, West Conshohocken, PA. https://doi.org/10.1520/D2435_D2435M-
718 25

719 ASTM (2025b) Standard test methods for particle-size distribution (gradation) of soils using sieve analysis (ASTM
720 D6913/D6913M-17(2025)). ASTM International, West Conshohocken, PA. https://doi.org/10.1520/D6913_D6913M-
721 17R25

722 ASTM (2026a) Standard test methods for liquid limit, plastic limit, and plasticity index of soils (ASTM D4318-26).
723 ASTM International, West Conshohocken, PA. https://doi.org/10.1520/D4318-26

724 ASTM (2026b) Standard test methods for downhole seismic testing (ASTM D7400/D7400M-26). ASTM International,
725 West Conshohocken, PA. https://doi.org/10.1520/D7400_D7400M-26

726 Bedin J, Schnaid F, Viana da Fonseca A, Costa Filho LM (2012) Gold tailings liquefaction under critical state soil
727 mechanics concepts. Géotechnique 62(3):263–267. https://doi.org/10.1680/geot.10.P.037

728 Cacciuttolo C, Valenzuela F (2022) Efficient use of water in tailings management: new technologies and environmental
729 strategies. Water 14:1741. https://doi.org/10.3390/w14111741

730 Carneiro JJV (2021) Characterization and behaviour of iron ore tailings: the effect of compaction and stresses. MSc
731 thesis, Universidade Federal de Viçosa, Viçosa

732 Carneiro JJV, Marques EAG, Viana da Fonseca AJP et al (2023) Characterization of an iron ore tailing sample and
733 evaluation of its representativeness. Geotech Geol Eng 41:2833–2852. https://doi.org/10.1007/s10706-023-02430-8

Carrera A, Coop M, Lancellotta R (2011) Influence of grading on the mechanical behaviour of Stava tailings. Géotechnique 61:935–946. https://doi.org/10.1680/geot.9.P.009

Carvalho JA, Wagner AC, Scheuermann Filho HC, Consoli NC (2024) The role of fabric, stress history, mineralogy and particle morphology on triaxial behaviour of non-textbook geomaterials. J Geotech Geoenviron Eng 150:04024055. https://doi.org/10.1061/(ASCE)GT.1943-5606.0003199

Cavalcanti JAD, Silva MS, Schobbenhaus C, Atencio D, Lima HM (2023) Geoconservation of geological and mining heritage related to banded iron formation. Int J Geoherit Parks 11:118–148. https://doi.org/10.1016/j.ijgeop.2022.12.002

Ccotohuanca J, Lanza V, Costa I (2024) The critical state line parameters of iron ore tailings from basic laboratory tests. In: Proceedings of the International Conference on Soil Mechanics and Geotechnical Engineering, ISSMGE

Chicot D, Mendoza J, Zaoui A, Louis G, Lepingle V, Roudet F, Lesage J (2011) Mechanical properties of magnetite, hematite and goethite by indentation and molecular dynamics. Mater Chem Phys 129:862–870. https://doi.org/10.1016/j.matchemphys.2011.05.056

Cho GC, Dodds J, Santamarina JC (2006) Particle shape effects on packing density, stiffness and strength. J Geotech Geoenviron Eng 132:591–602. https://doi.org/10.1061/(ASCE)1090-0241(2006)132:5(591)

Chu J, Wanatowski D (2008) Instability conditions of loose sand in plane strain. J Geotech Geoenviron Eng 134:136–142. https://doi.org/10.1061/(ASCE)1090-0241(2008)134:1(136)

Consoli NC, Carvalho JVA, Wagner AC, Silva JPS, Cacciari PP (2024a) Determination of critical state line (CSL) for silty-sandy iron ore tailings subjected to low–high confining pressures. J Rock Mech Geotech Eng 16:1684–1695. https://doi.org/10.1016/j.jrmge.2023.06.014

Consoli NC, Silva JPS, Wagner AC, Carvalho JVA, Baudet BA, Coop M, Scheuermann Filho HC, Carvalho I, Sousa GM, Cacciari PP (2024b) Critical state analysis of two compacted filtered iron ore tailings with different gradings and mineralogy at different stages of treatment. Acta Geotech 19:881–898. https://doi.org/10.1007/s11440-023-01963-9

Consoli NC, Wagner AC, Gonçalves TM, Vizcarra GOC, Pereira F, Carvalho JVA (2025) Evaluation of iron ore tailings during dam closure using instrumentation, field testing and numerical modelling. Geotech Geol Eng 43:346. https://doi.org/10.1007/s10706-025-03302-z

Coop M (1999) On the mechanics of reconstituted soils. In: Proceedings of the International Workshop on Characterization and Engineering Properties of Natural Soils, vol 1. Balkema, Rotterdam, pp 313–338

Coop M (2004) The mechanics of granular soils: critical state, structure and fabric. In: Proceedings of the Skempton Memorial Conference, vol 1. Thomas Telford, London, pp 297–324

Coop M, Airey D (2003) Soil behaviour and critical state soil mechanics. Proc Inst Civ Eng Geotech Eng 156:134–141

Corrêa de Oliveira S, Delgado BG, Paes IT, Viana da Fonseca A, Pereira EL, Paes BST (2025) Influence of stress state on the expected behaviour of filtered iron ore tailings for compacted stacking disposal. Geotech Test J 48:166–189. https://doi.org/10.1520/GTJ20230503

Coutinho RS, Silva RSA, Almeida MSS, Cavalcanti MCR, Nagula SS, Delgado BG (2025) Static liquefaction susceptibility of a Brazilian iron ore tailings dam: a combined laboratory testing and numerical modelling approach. Int J Geomech 25:04025167. https://doi.org/10.1061/IJGNAI.GMENG-11018

De Andrade RB, Silva RSA, Almeida MSS, Nagula SS (2025) Evaluation of the liquefaction potential of filtered tailings stacks by means of laboratory investigation. Can Geotech J 62:1–13. https://doi.org/10.1139/cgj-2024-0274

Delgado BG, Viana da Fonseca A, Bittar RJ, Castilho BM, Coelho D (2023) Geomechanical behaviour of iron ore tailings under high stress levels for disposal by dry stacking. In: Proceedings of the 1st International Conference on Geotechnics of Tailings and Mine Waste, Ouro Preto

Delgado BG, Viana da Fonseca A, Bittar RJ, Besenzon D, Molina-Gómez F, Cordeiro D, Mendonça A, Rios S (2025) Critical state loci of superheavy iron ore tailings from sampling in Brumadinho reservoir. J Geotech Geoenviron Eng 151:04025104. https://doi.org/10.1061/JGGEFK.GTENG-13055

778 Dias Neto SLS, Ferraz RL, Silva TO, Marques EAG, Pitanga HN, Cândido ES (2024) Hydraulic characteristics of silt-
779 sized iron ore tailings. Geotech Geol Eng 42:3731–3753. https://doi.org/10.1007/s10706-024-02755-y

780 Dias Neto SLS, Ferraz RL, Silva TO, Marques EAG, Pitanga HN, Cândido ES (2025) Numerical evaluation of hydraulic
781 and stability responses in filtered tailings stacks under variable construction conditions. Geotech Geol Eng 43:337.
782 https://doi.org/10.1007/s10706-025-03321-w

783 Dos Santos VC, Rubinger T, Almeida M, Silva D, Oliveira M, Rodrigues A, Pereira J, Barbosa F, Malm O (2020) Metal
784 concentrations and biological effects from one of the largest mining disasters in the world (Brumadinho, Brazil). Sci
785 Rep 10:5936. https://doi.org/10.1038/s41598-020-62700-w

786 Eloi DM (2021) Ensaios triaxiais com procedimentos convencionais e avançados para avaliação de estados críticos em
787 rejeitos de ferro. MSc thesis, Universidade do Porto

788 Faria AO (2022) Avaliação comparativa de modelos constitutivos para um rejeito de minério de ferro do Quadrilátero
789 Ferrífero. MSc thesis, Universidade Federal de Ouro Preto

790 Faria, AO, Santos Junior MP, Delgado BG, Carneiro JJV, Pinto GHS (2024) Numerical simulation of the stress–strain
791 behaviour of an iron ore tailings from the Quadrilátero Ferrífero. In: Proceedings of COBRAMSEG 2024.
792 https://doi.org/10.47094/COBRAMSEG2024/475

793 Ferreira PMV, Bica AVD (2006) Problems in identifying the effects of structure and critical state in a soil with
794 transitional behaviour. Géotechnique 56:445–454. https://doi.org/10.1680/geot.2006.56.7.445

795 Finno RJ, Rechenmacher AL (2003) Effects of consolidation history on critical state of sand. J Geotech Geoenviron
796 Eng 129:350–360. https://doi.org/10.1061/(ASCE)1090-0241(2003)129:4(350)

797 Fletcher T, Chandan C, Masad E, Sivakumar K (2003) Aggregate imaging system for characterizing the shape of fine
798 and coarse aggregates. Transp Res Rec 1832:67–77. https://doi.org/10.3141/1832-09

799 Fourie AB, Tshabalala L (2005) Initiation of static liquefaction and the role of K_0 consolidation. Can Geotech J 42:892–
800 906. https://doi.org/10.1139/t05-026

801 Graham JP, Jefferies MG (1986) Some examples of in situ lateral stress determinations in hydraulic fills using the
802 selfboring pressuremeter. In: Proceedings of the 39th Canadian Geotechnical Conference, Ottawa, pp 1–14

803 Gunnteg M, Reid D, Fourie A (2025) Effects of sample preparation on NorSand calibration outcomes. In: Proceedings
804 of Tailings and Mine Waste 2025, Banff

805 Head KH (1982) Manual of soil laboratory testing. Vol 2: Permeability, shear strength and compressibility tests. Pentech
806 Press, London

807 ICOLD (2025) Tailings dam safety. ICOLD Bulletin 194. International Commission on Large Dams, Paris

808 Ishihara K (1996) Soil behaviour in earthquake geotechnics. Oxford University Press, Oxford

809 Islam K, Murakami S (2021) Global-scale impact analysis of mine tailings dam failures: 1915–2020. Glob Environ
810 Change 70:102361. https://doi.org/10.1016/j.gloenvcha.2021.102361

811 Jaky J (1944) The coefficient of earth pressure at rest. Journal of the Society of Hungarian Architects and Engineers,
812 78, 355–358

813 Jefferies MG, Been K (2016) Soil liquefaction: a critical state approach, 2nd edn. Taylor & Francis, London

814 Jefferies MG, Shuttle DA (2002). Dilatancy in general Cambridge-type models. Géotechnique, 52(9), 625–638.
815 https://doi.org/10.1680/geot.2002.52.9.625

816 Ji X, Xu Q, Ren K, Wei L, Wang W (2024) Critical state analysis for iron ore tailings with a fine-grained interlayer:
817 effects of layering thickness and dip angle. Water 16:1488. https://doi.org/10.3390/w16101488

818 John NJ, Khan I, Kandalai S, Patel A (2023) Particle breakage in construction materials: A geotechnical perspective.
819 Construction and Building Materials 381:131308. https://doi.org/10.1016/j.conbuildmat.2023.131308

820 JSCE (2009) Test method for maximum and minimum density of sands (JSCE-G 582). Japan Society of Civil Engineers,
821 Tokyo

822 Ladd RS (1978) Preparing test specimens using undercompaction. In: Proceedings of Symposium on Recent
823 Developments in Soil Mechanics. ASCE, pp 1–23

824 Lade PV, Trads N (2014) The role of cementation in the behaviour of cemented soils. Geotech Res 1:111–132

825 Lashkari A, Falsafizadeh SR, Shourijeh PT, Alipour MJ (2020) Instability of loose sand in constant volume direct simple
826 shear tests in relation to particle shape. Acta Geotech 15:2507–2527. https://doi.org/10.1007/s11440-019-00909-4

827 Lyu Z, Chai J, Xu Z, Qin Y, Cao J (2019) A comprehensive review on reasons for tailings dam failures based on case
828 history. Adv Civ Eng 2019:4159306. https://doi.org/10.1155/2019/4159306

829 Macedo J, Vergaray L (2022) Properties of mine tailings for static liquefaction assessment. Canadian Geotechnical
830 Journal 59(5): 667–687. https://doi.org/10.1139/cgj-2020-0600

831 Marsal R (1967) Mechanical properties of soils under various conditions of stress. National Academy of Sciences,
832 Washington, DC

833 Morgenstern NR, Vick SG, Viotti CB, Watts BD (2016) Fundão tailings dam review panel: Immediate causes of the
834 failure of the Fundão Dam. Technical report, Cleary Gottlieb Steen & Hamilton LLP, New York

835 Nocilla A, Coop M, Colleselli F (2006) The mechanics of an Italian silt: an example of transitional behaviour.
836 Géotechnique 56:261–271. https://doi.org/10.1680/geot.2006.56.4.261

837 Oliveira ÂHC (2021) Stress–strain analysis in a large-scale filtered tailings stack. MSc thesis, Universidade Federal de
838 Viçosa, Viçosa, Brazil

839 Pacheco Silva A (1970) O comportamento tensão–deformação dos solos argilosos e sua importância nas obras de
840 engenharia. Solos e Rochas 3:83–96

841 Pestana JM (1996) A unified description of soil behavior. In: Lin YK, Su TC (eds) Proceedings of the 11th Engineering
842 Mechanics Conference. ASCE, pp 281–284

Ponzoni E, Nocilla A, Coop M, Colleselli F (2014) Identification and quantification of transitional modes of behaviour in sediments of Venice lagoon. Géotechnique 64:694–708. https://doi.org/10.1680/geot.13.P.166

Rabbi ATMZ, Rahman MM, Cameron DA (2018) Undrained behavior of silty sand and the role of isotropic and K_0 consolidation. J Geotech Geoenviron Eng 144:04018014. https://doi.org/10.1061/(ASCE)GT.1943-5606.0001859

Reid D, Fourie A, Ayala JL, Dickinson S, Ochoa-Cornejo F, Fanni R, Garfias J, Fonseca AV, Ghafghazi M, Ovalle C, Riemer M, Rismanchi A, Olivera R, Suazo G (2020) Results of a critical state line testing round robin programme. Géotechnique 70:616–630. https://doi.org/10.1680/jgeot.19.P.373

Reid D, Fourie A, Dickinson S, Shanmugarajah T, Fanni R, Smith K, Garfias J, Yuan B, Ghafghazi M, Duyvestyn A (2025) Results of a dilatancy round robin. Geotech Res 12:2–28. https://doi.org/10.1680/jgere.24.00008

Rios S, Ciantia M, Gonzalez N, Arroyo M, Viana da Fonseca A (2016) Simplifying calibration of bonded elasto-plastic models. Comput Geotech 67:100–108. https://doi.org/10.1016/j.compgeo.2015.12.001

Rios S, Viana da Fonseca A, Caetano I, Delgado B, Pereira G (2025) Comparison of geomechanical behavior of an iron ore tailings and natural siliceous silty sand with the same particle size distribution. Can Geotech J 62. https://doi.org/10.1139/cgj-2025-0215

Robertson PK, de Melo L, Williams DJ, Wilson GW (2019) Report of the expert panel on the technical causes of the failure of Feijão Dam I. Technical report, Vale

Roscoe KH, Schofield AN, Wroth CP (1958) On the yielding of soils. Géotechnique, 8(1):22–53. https://doi.org/10.1680/geot.1958.8.1.22

Santana F (2022) Estudo do comportamento geomecânico de rejeitos de minério de ferro em ensaios triaxiais. MSc thesis, Universidade do Porto, Faculdade de Engenharia, Porto, Portugal

Schnaid F, Bedin J, Viana da Fonseca AJP, Costa Filho LM (2013) Stiffness and strength governing the static liquefaction of tailings. Journal of Geotechnical and Geoenvironmental Engineering 139(12):2136–2144. https://doi.org/10.1061/(ASCE)GT.1943-5606.0000924

866 Shuttle D, Jefferies M (2005) NorSand: description, calibration, validation and applications. Technical report

867 Silva JPS, Carvalho JVA, Wagner AC, Cacciari PP, Consoli NC (2024a) On the mechanics of filtered compacted
868 consolidated and overconsolidated iron ore tailings at high pressures. Can Geotech J 61:575–581.
869 https://doi.org/10.1139/cgj-2023-0056

870 Silva JPS, Rissoli ALC, Cacciari PP, Viana da Fonseca A, Filho HCS, Wagner AC, Carvalho JVA, Festugato L, Consoli
871 NC (2024b) Triaxial testing response of compacted iron ore tailings considering a broad spectrum of confining
872 pressures. Soils Found 64:101438. https://doi.org/10.1016/j.sandf.2024.101438

873 Skempton AW (1954) The pore-pressure coefficients A and B. Géotechnique 4:143–147.
874 https://doi.org/10.1680/geot.1954.4.4.143

875 Terzaghi K, Peck RB, Mesri G (1996) Soil mechanics in engineering practice, 3rd edn. John Wiley & Sons, New York

876 Torres-Cruz LA (2019) Limit void ratios and steady-state line of non-plastic soils. Proc Inst Civ Eng Geotech Eng
877 172:235–246. https://doi.org/10.1680/jgeen.18.00011

878 Torres-Cruz LA, Santamarina JC (2020) The critical state line of non-plastic tailings. Can Geotech J 57:1508–1517.
879 https://doi.org/10.1139/cgj-2019-0019

880 Velten RZ, Ulsen C, da Costa JPR, Lima CAA, Mafessoli M, Carvalho JVA, Consoli NC (2025) Role of mineralogy
881 on the undrained monotonic simple shear response of compacted filtered copper tailings. Soils Found 65:101636.
882 https://doi.org/10.1016/j.sandf.2025.101636

883 Verdugo R (1992) Characterization of the shear behavior of sands. PhD thesis, University of Illinois at Urbana–
884 Champaign, Urbana, IL, USA

885 Viana da Fonseca A (2026) The 10th James K. Mitchell Lecture – In situ and lab tests work together to reduce
886 uncertainties in TSF fragility assessment: a benchmark case-history. Soils Rocks.
887 https://doi.org/10.28927/SR.2026.011425

888 Viana da Fonseca A, Cordeiro D, Molina-Gómez F (2021) Recommended procedures to assess critical state locus from
889 triaxial tests in cohesionless remoulded samples. Geotechnics 1:95–127. https://doi.org/10.3390/geotechnics1010006

890 Viana da Fonseca A, Cordeiro D, Molina-Gómez F, Besenzon D, Fonseca A, Ferreira C (2022) The mechanics of iron
891 tailings from laboratory tests on reconstituted samples collected in post-mortem Dam I in Brumadinho. Soils Rocks
892 45:e2022001122. https://doi.org/10.28927/SR.2022.001122

893 Viana da Fonseca A, Molina-Gómez F, Besenzon D, Coelho D (2023) The influence of stress-induced anisotropy in
894 undrained yield and ultimate shear strengths in brittle loose silts. In: Proceedings of the 8th International Symposium
895 on Deformation Characteristics of Geomaterials (ISDCG 2023), Porto, Portugal

896 Viana da Fonseca, A.J.P. & Delgado, B.G. (2026) Improving the sustainability of tailings disposal through better
897 practices in filtered tailings stacks. In: Fourie, A.B., Horta, M., Oliveira, M. & Wilson, S. (eds.), Paste 2026: Proceedings
898 of the 27th International Conference on Paste, Thickened and Filtered Tailings, Lisbon, Portugal, pp. 1–20. Australian
899 Centre for Geomechanics, Perth. https://doi.org/10.36487/ACG_repo/2655_0.02

900 Vick SG (1990) Planning, design, and analysis of tailings dams, 2nd edn. BiTech Publishers, Vancouver

901 Xu L, Coop M (2017) The mechanics of a saturated silty loess with a transitional mode. Géotechnique 67:581–596.
902 https://doi.org/10.1680/jgeot.16.P.128

903 Wagner AC, Carvalho JVA, Scheuermann Filho HC, Consoli NC (2025) Influence of grading in compacted tailings
904 behaviour: towards resilient design. Géotechnique 75:150–163. https://doi.org/10.1680/jgeot.23.00475

905 Yang Y, Wei Z, Fourie AB, Chen Y, Zheng B, Wang W, Zhuang S (2019) Particle shape analysis of tailings using
906 digital image processing. Environ Sci Pollut Res 26:26397–26403. https://doi.org/10.1007/s11356-019-05964-9

907 Zhang JX (2023) Research on the relationship between international trade and economic development and the
908 environment. Bus Exhib Econ 2023:75–78. https://doi.org/10.19995/j.cnki.CN10-617/F7.2023.11.075

Supplementary Files

This is a list of supplementary files associated with this preprint. Click to download.

- Supplementary1.docx
- Supplementary2.docx